Development of Electron Beam Model in TOPAS through Iterative Modeling of Clinical Data

By

Forrest Ivey

A THESIS

Presented to the Department of Medical Physics

and the Oregon Health & Science University

School of Medicine

in partial fulfillment of

the requirements for the degree of

Master of Science

June 2021

TABLE OF CONTENTS

List of Figures ..... **iii**

List of Tables ..... **vi**

Acknowledgments ..... **vii**

Abstract ..... **viii**

1. Introduction **1**

2. Background **2**

2.1. Electron Beam Therapy 2

2.2. Monte Carlo Method 7

2.2.1. TOPAS MC HISTORY 10

2.3. AIM OF THE STUDY 11

3. Methods **13**

3.1. TOPAS MC Simulations 13

3.2. Electron Beam Simulation 13

3.2.1. Gantry Head Geometry 15

3.2.2. Primary Collimator 19

3.2.3. Primary and Secondary Scattering Foils 19

3.2.4. Electron Cone Applicators 22

3.2.5. Data Acquisition Through Scoring 23

3.2.6. Iteration & the Graphical User Interface 25

4. Results **28**

4.1. Modeled Components 28

4.1.1. Component Placement 28

4.1.2. Primary Collimator 28

4.1.3. MLC and Jaws 29

4.1.4. Electron Cones 31

4.1.5. Secondary Scattering Foil 34

4.2. Final Model 38

5. Discussion 41

5.1. Complete Model 41

5.2. Model Limitations 42

5.3. Future Work 43

5.4. Conclusion 44

6. Conclusion 45

7. References 46

8. Appendix 48

8.1. Iterative Process 48

8.2. Graphs 50

List of Figures

Figure 1. Thorough depiction of a modern medical linear accelerator that is set up for an electron beam treatment. 3

Figure 2. An Elekta Versa HD electron cone system for treating a 10 by 10-cm^2 field size with labeled components and axis. 7

Figure 3. Example of a probability distribution to characterize discrete events and associate an outcome through the use of random number generation between zero and one. 9

Figure 4. The layout of the TOPAS expansion of the Geant4 toolkit with an example user parameter file and ability to stack parameter files within a file hierarchy system. 11

Figure 5. The layout of the BEAM model for the Varian Clinac 2100C linear accelerator used to simulate electron beams. This was used as a basis for determining component sizes and location placement within the TOPAS simulation. 16

Figure 6. Model of the Elekta Versa HD linear accelerator gantry head developed within BEAMnrc from information provided to the original created through a non-disclosure agreement. Used for the creation of the final model, determining component sizes, and location placement within the TOPAS simulation. 18

Figure 7. Depiction of how a dual-scattering foil system works to flatten the Gaussian distribution produced by the primary scattering foil. 20

Figure 8. Secondary scattering foil design made of 10 cylindrical disks for a 6 MeV electron beam. 21

Figure 9. Electron Cone applicator layout for an Elekta SLi Plus linear accelerator built within the Monte Carlo code BEAMnrc. 23

Figure 10. Water Phantom projection showing the axes and orientation of the incident beam. 24

Figure 11. A screenshot of the off-axis profile tab within the graphical user interface. 25

Figure 12. A screenshot of the percent depth dose profile tab within the graphical user interface. 26

Figure 13. A screenshot of a section analysis of the primary collimator created within Autodesk® Fusion 360™ 29

Figure 14. A screenshot of the multi-leaf collimator block and Y-diaphragm created within Autodesk® Fusion 360™. 31

Figure 15. A screenshot of the 10 by 10 cm^2 field size electron cone created within Autodesk® Fusion 360™. 33

Figure 16. A screenshot of the 10 by 10 cm^2 electron cone system created within TOPAS using basic geometry components. 34
Figure 17. The total sum difference between each point of the simulation data and the clinical data within different locations of the off-axis profile for the 6 MeV energy electron beam at a depth of 1.4 cm and 10 by 10 cm^2 field size. The blue bar is data from version 1.19 with a 0.255 cm secondary scattering foil thickness and the red bar is from version 1.18 with a 0.3 cm secondary scattering foil which both use the TOPAS built electron cone. The yellow bar is data from version 1.17 with a 0.255 cm secondary scattering foil and the purple bar is version 1.16 with a 0.26 secondary scattering foil thickness which both use the imported electron cone. 35
Figure 18. The off-axis profile for comparison of the 2 billion history count simulation for the final version of the model, which uses a 0.255-centimeter secondary scattering foil thickness, for a 10 by 10 cm^2 field size versus the clinical data at a depth of 1.4 centimeters. 36
Figure 19. The percent depth dose curve for comparison of the 2 billion history count simulation for the final version of the model, which uses a 0.255-centimeter secondary scattering foil thickness, for a 10 by 10 cm^2 field size versus the clinical measured data. 37
Figure 21. A screenshot of the final electron beam model minus the gantry shielding cover is shown in the graphical display settings within TOPAS. 39
Figure 22. A zoomed-in shot of the final electron beam model to showcase the small primary scattering foil located above the primary collimator. 40
Figure 23. The graph between versions V1.17 and V1.19 where a new applicator system was created through the use of basic geometry figures built-in to the TOPAS software. 50
Figure 24. Zoomed in screenshot of the off-axis profiles between versions V1.17 and V1.19, where a new applicator system was created. This shows the spike in the off-axis profile located outside of the penumbral region. 51
Figure 25. The total sum difference between each point of the simulation data and the clinical data within the tail of the off-axis profile between -11.3 and -5.8 cm for the 6 MeV energy electron beam at a depth of 0.95 cm and 10 by 10 field size. 52
Figure 26. The total sum difference between each point of the simulation data and the clinical data within the penumbra of the off-axis profile between -5.8 and -4.85 cm for the 6 MeV energy electron beam at a depth of 0.95 cm and 10 by 10 field size. 53

Figure 27. The total sum difference between each point of the simulation data and the clinical data within the middle section of the off-axis profile between -4.85 and 4.85 cm for the 6 MeV energy electron beam at a depth of 0.95 cm and 10 by 10 field size. 54
Figure 28. The total sum difference between each point of the simulation data and the clinical data within the penumbra of the off-axis profile between 4.85 and 4.75 cm for the 6 MeV energy electron beam at a depth of 0.95 cm and 10 by 10 field size. 55
Figure 29. The total sum difference between each point of the simulation data and the clinical data within the tail of the off-axis profile between 4.75 and 11.3 cm for the 6 MeV energy electron beam at a depth of 0.95 cm and 10 by 10 field size. 56
Figure 30. The total sum difference between each point of the simulation data and the clinical data within the off-axis profile for the 6 MeV energy electron beam at a depth of 0.95 cm and 10 by 10 field size. .. 57

List of Tables

Table 1. The atomic weight fractions used in the formation of a mild steel material within TOPAS. 22

Table 2. Bin numbers used in the water phantom for scoring of dose deposition. 24

Table 3. The distance from the exit window of the simulation to the top of each component that was modeled within the system. 28

Table 4. Dimensions calculated for the creation of the primary collimator. 29

Table 5. The dimensions calculated through ImageJ from the Varian Clinac 2100C used in the creation of the MLC/Y-Diaphragm components. 30

Table 6. The dimensions calculated through ImageJ from the Elekta Versa HD used in the creation of the MLC/Y-Diaphragm components. 30

Table 7. Dimensions of each scraper measured from the Elekta Versa HD electron cones used in the clinic. 32

Table 8. Distance between each scraper set measured from the Elekta Versa HD electron cones used in the clinic. 32

Acknowledgments

I would like to express my gratitude to my mentor and chair, Dr. Richard Crilly and Dr. Kyle Gallagher, for being a fantastic resource of ideas and advice. They helped me find solutions to any issues that I faced and helped guide me on the physics behind the answers.

Thank you to my cohort, Alyssa, Austin, Bailey, Grace, Homa, Jacob, and John, for their help and friendship throughout these last two years. I would also like to thank the rest of the faculty involved with the medical physics program at OHSU for their guidance and teachings.

Lastly, I would like to thank my family & my dog Onyx for helping me pursue my goals of obtaining a Master's degree in Medical Physics and becoming a clinical radiation physicist. Your support has been and will continue to be genuinely appreciated.

Abstract

Purpose: To create an electron beam model with an energy of 6 MeV in the Monte Carlo code TOPAS through open-source data and papers that is comparable to clinical data for future computational electron research and clinical development.

Methods: One way to accomplish electron beam research is to use computational models based on solutions of Monte Carlo codes to the transport equation. The first step in any computational research project is creating the initial beam model, which should be validated with acquired measurements from clinically relevant fields. For the sake of expediency, an iterative modeling process was performed. Information regarding the size and composition of each component modeled within the simulation needed to be acquired from open-source data. From the figures, dimensions, location placement, and material composition for each component were determined. The iterative process played a more prominent role for the secondary flattening filter due to its Gaussian shape to flatten the particle distribution created by the primary scattering foil. Clinical measured data of a 6 MeV electron beam from an Elekta Versa HD was used to compare the electron beam model created within TOPAS through the development of a graphical user interface. Measurements were taken from the 6, 10, 14, 20, and 25 cm field electron cones.

Results: Using this method, a 6 MeV electron beam model was created in TOPAS and compared to clinical data from an Elekta Versa HD linear accelerator. Models were created for the primary scattering foil, primary collimator, secondary scattering foil and holder, MLC blocks, secondary jaw blocks, gantry faceplate, and electron beam applicators. The secondary scattering foil thickness of 0.255 centimeters was determined to produce an adequate off-axis profile with the full width at half maximum differing by 1.29% and a flatness difference of 3.41%. Compared to the clinical data, the percent depth dose curve has a large difference with R_{90} and R_{50} differ by 36.88% and 14.33%, respectively. However, this is more

representative of a 5 MeV electron beam. Several iterations were performed to reach the final model, with the graphical user interface producing plots to allow for easy comparison between clinical data and data acquired from the simulations.

Conclusion: As an initial project that will be a foundation point for future studies, it showed that the iterative process could create a model of an electron beam comparable to clinical data. With enough time and resources, more models could be made for energies other than 6 MeV. However, further investigation should be completed to minimize the leakage radiation caused by the applicator system to achieve clinically accurate off-axis dose profiles.

1. Introduction

It is estimated that 1.9 million people will be diagnosed with cancer in the United States during 2021, to which approximately 609,000 of those diagnosed will die from their cancer.[1] Electron radiation therapy has been used as a form of treatment for many superficial cancers such as skin, lip, breast, total skin, and head and neck cancers. Electron therapy offers a wide variety of treatment energies, exhibits a steep dose falloff and higher surface dose, making it a viable option for superficial cancers. These qualities help minimize the dose received by critical structures located deeper than the area being treated.[2]

Prior to this thesis research, Oregon Health & Science University did not have any research-based computational model related to electron therapy treatments. The purpose of this thesis is to create a computational model that is comparable to measured clinical data. At this time, Oregon Health & Science University only perform electron beam therapy treatments through an Elekta Versa HD linear accelerator. (Elekta Versa HD, Elekta Oncology Systems, Crawley, United Kingdom) This linear accelerator was commissioned for electron and photon therapy treatments, but for the purposes of this study, only the electron portion will be considered. For universities or institutions with models of their systems, most approach vendors and receive non-disclosure agreements to obtain proprietary data on the components within the linear accelerator. This process was deemed too time consuming to be done within temporal confines of a M.Sc. thesis. However, with a functional model, it would be possible to test experimental research without performing physical experiments. The rest of this paper will address the methods for creating this model and the limitations discovered along the way.

2. Background

2.1. Electron Beam Therapy

In the late 1930's two MIT professors, Van de Graaff and Trump, developed the Van de Graaff accelerator. This system produced an electron beam of energy less than 3 MeV, which limited its use to primarily mycosis fungoides and types of skin cancers. In the 1940s, shortly after creating the Van de Graaff accelerator, the Betatron was created.[3] These systems were capable of producing an energy range between 6 and 30 MeV and gained a more prominent role in the clinic as companies such as Siemens, Brown Boveri, and Allis Chalmers made them more readily available. These two systems paved the way for creating the linear accelerator in the 1960s, which along with Co-60 units, began to phase out orthovoltage x-ray machines. Modern-day linear accelerators have the ability to deliver both electron and photon treatments providing multiple treatment opportunities for patients.

Modern linear accelerators treat patients with a gantry system that can rotate around the patient. Most components needed to create the electron beam are located within the gantry, and the beam is shaped within the gantry head. An example of the components used for creating an electron beam is illustrated in **Figure 1**. Beam formation utilizes the fundamental concepts of an

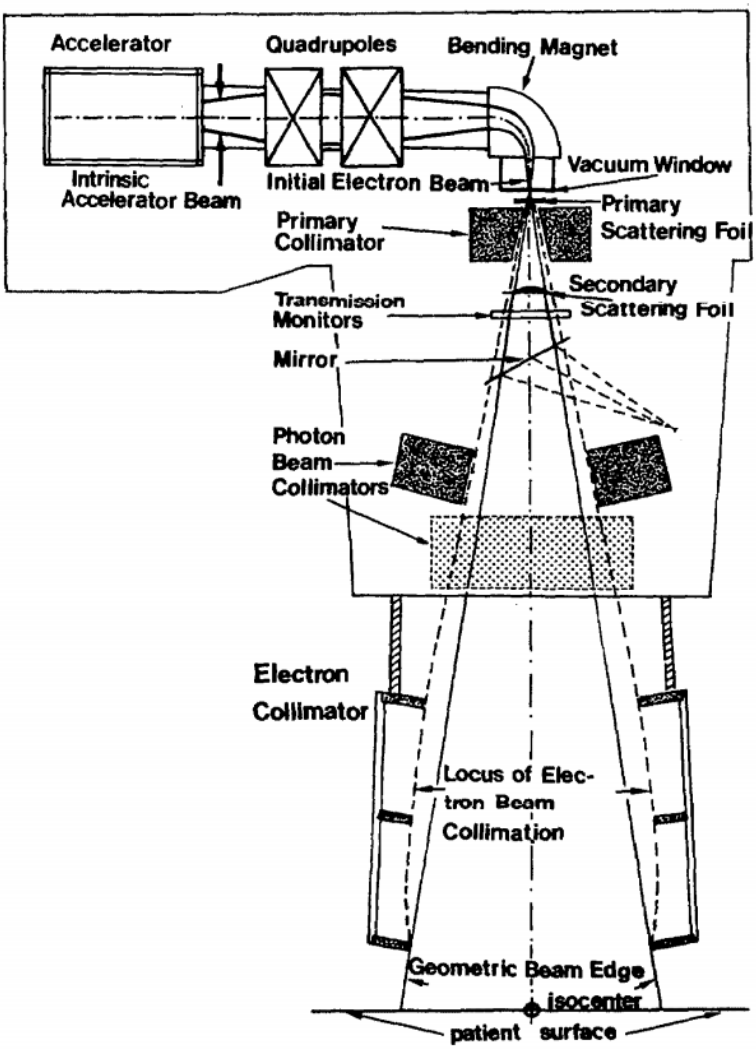

Figure 1. Thorough depiction of a modern medical linear accelerator that is set up for an electron beam treatment. Reproduced with permission of the International Commission on Radiation Units and Measurements, https://www.icru.org/

x-ray tube but work to increase the beam's kinetic energy through additional components within a vacuum environment.[4] At the electron gun, a filament is stripped of electrons through thermionic emission, which are injected into the accelerating waveguide. In conjunction with high-power microwaves created by either a magnetron or klystron, electrons are accelerated in an accelerator tube to increase their energy to the megavoltage range. The magnetron has a cylindrical shape with a central cathode, an outer copper anode with resonant cavities, a static magnetic field applied perpendicular to the cavities, and a pulsed DC electric field between the

cathode and anode. The cathode is heated to strip off electrons through thermionic emission, which interact with the magnetic field and travel in complex spirals around the resonant cavities generating microwaves that can be used within the accelerating waveguide. Unlike the magnetron, the klystron amplifies microwaves rather than generating them and is driven by a low-power microwave oscillator. The microwaves are injected into the klystron generating an alternating electric field across the cavity that alters the velocity of electrons injected into the klystron. The electrons bunch into groups within the drift tube and travel towards the catcher cavity; it induces charges at the end of the cavity that generates an electric field. The electrons are decelerated, causing the kinetic energy to be converted into high-power microwaves that are input into the accelerating waveguide.

The electrons injected from the electron gun travel one to two meters to the end of the accelerating waveguide, where they enter the linear accelerator's head.[5] With the magnetron, the energy of the electrons at the end of the accelerating waveguide is dependent on the radiofrequency power and the electron beam current. The magnitude of the radiofrequency power is dependent on the input power to the magnetron. For an Elekta linear accelerator, the electron beam changes direction through the use of an elaborate slalom design bending magnet consisting of two 45° and one 112.5° bending magnets. Most of the electrons are nearly monoenergetic and converge to a small point forming a pencil beam that can then be used as the basis for treatment beam formation. The electron beam leaves the vacuum environment through a metal exit window, typically made of nickel. It then interacts with the primary scattering foil, a high-Z material of uniform thickness, such as Tungsten or Tantalum. The scattered pencil beam becomes a broadened electron beam that holds an approximately radial Gaussian distribution. A secondary scattering foil made of a low-Z material, such as aluminum or zinc alloy, of varying thickness is the next component the electrons pass through. A broad and flat beam is produced

when both the primary and secondary scattering foils are used.[4] Together, it is not possible for one combination of a primary and secondary scattering foil to create a broad and flat beam for various beam energies. Due to this, linear accelerator vendors have multiple thicknesses of primary and secondary scattering foils that are combined to work for all clinically available beam energies. For electrons, collisional and radiation stopping powers are dependent on the atomic number of the material that each particle interacts with. The collisional stopping power for high-energy electrons decreases as the atomic number increases; however, this decrease reduction is less than a factor of two. The energy loss due to collisional processes is a stochastic process. For a monoenergetic beam, these collisions will result in a spread-out gradient distribution that makes this an important factor in the material selection of the primary scattering foil. The radiative stopping power has a Z^2 dependence and is the rate of energy loss that results in the production of bremsstrahlung radiation. For high-Z materials, radiation stopping power begins to dominate at approximately 10 MeV, and for low-Z materials, it dominates around 100 MeV. Using a lower-Z material for the secondary scattering foil helps to ensure bremsstrahlung contamination is minimized.

Two ionization chambers are located directly beneath the secondary scattering foil to monitor the radiation that is being delivered by the system. A collection of secondary collimators are placed outside the beam at varying field sizes based on the electron cone attached to the gantry head. One reason for this, the collimators are made from high-Z material that will cause increased secondary scatter radiation that can interact with the patient resulting in a higher surface dose to the patient. The mean energy of the scattered electrons is roughly 40% of the mean energy of the beam.[6] This scattered radiation, along with photon contamination, increases the treatment beam's geometric penumbra near the field edges. For an Elekta Versa HD, the

upper secondary collimator is the multi-leaf collimators (MLC), and the Y-diaphragm jaws represent the lower secondary collimator.

Due to the increased scatter contribution by the secondary collimator systems, electron beams require the use of an electron cone system to reduce the penumbra of the beam. Electron cones shape the electron beam through the use of layered scrapers that attach directly to the gantry head through a latching or sliding mechanism. Typically, ending five centimeters from the patient's surface, an insert can be placed within the collimator to provide further field definition using standard cutout or patient-specific shapes. An example of the electron cone used for the Elekta Versa HD is in **Figure 2**.

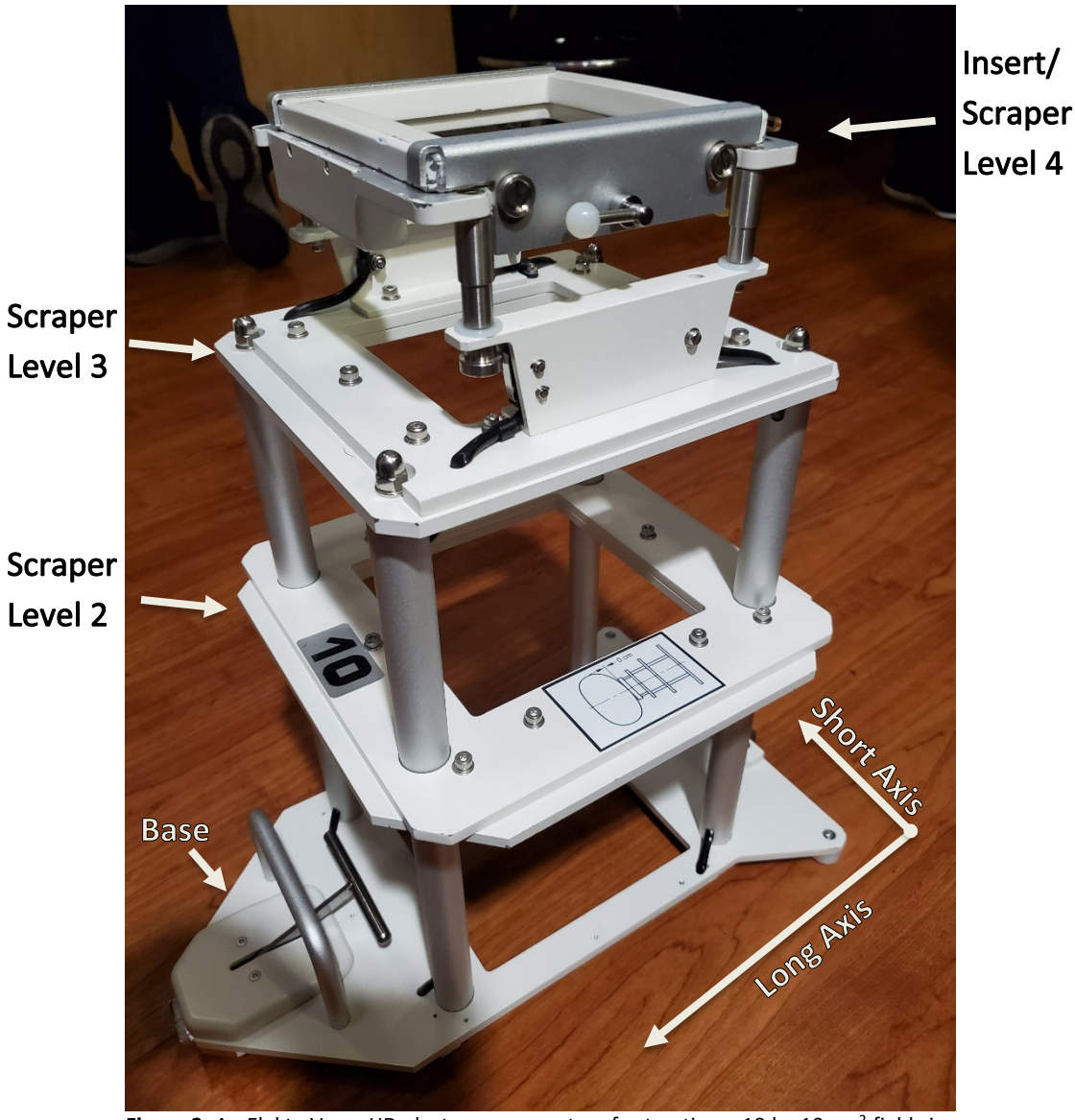

Figure 2. An Elekta Versa HD electron cone system for treating a 10 by 10-cm^2 field size with labeled components and axis.

2.2. Monte Carlo Method

Monte Carlo software was first developed and used during the Manhattan project as a means to calculate particle transport in a simulation processes. Shortly after, John von Neumann and Stanislaw Ulam suggested it would be a valuable tool to investigate neutron travel through radiation shielding and eventually named it after the Monte Carlo Casino in Monaco.[7] The simulation processes were used to predict the probability of unique outcomes when complex boundary conditions inhibit the ability to solve the problem through analytic means. These

predictions work by assigning a random value to the variable defined within a known probability distribution and then allowing the simulation to run. This process is repeated multiple times while randomly changing the value assigned to the variable that has uncertainty. For radiation physics, the software estimates characteristics of particle populations by predicting the probability of particle interactions to create solutions to the Boltzmann transport equation. It's not uncommon for transport problems to be incredibly complex when three-dimensional geometries or time-dependent values are incorporated for direct numerical solutions. This is where large random sampling methods can be used to estimate the expected behavior of a population of particles to solve the transport equation. (**Equation 1**)

$$\vec{\Omega} \cdot \vec{\nabla} N + \mu N = \int_{E}^{\infty} \int_{4\pi} N\left(\vec{r}, \vec{\Omega}', E'\right) K\left(\vec{r}, \vec{\Omega}' \rightarrow \vec{\Omega}, E' \rightarrow E\right) \cdot d\vec{\Omega}' dE' + S(\vec{r}, \vec{\Omega}, E) \qquad (1)$$

Where $\vec{r}$ is the three spatial coordinates, $\vec{\Omega}$ is the two-directional coordinates, E is the energy, $N\left(\vec{r}, \vec{\Omega}', E'\right) d\vec{\Omega}' dE'$ is the number of particles moving within a solid angle $d\Omega$ in a direction $\vec{\Omega}$ with a set energy range dE', $K\left(\vec{r}, \vec{\Omega}' \rightarrow \vec{\Omega}, E' \rightarrow E\right)$ is the scattering kernel showing the probability a particle will scatter into a set direction, Ω', and energy, E', and lastly, $S(\vec{r}, \vec{\Omega}, E)$ represents the source of the particles.[8] To show how the Monte Carlo software utilizes random number generation to solve the Boltzmann transport equation, here is a simple example represented by an electron beam that is incident on a water phantom in a cubical shape. The system first samples a random number between 0 and 1, then using the necessary attenuation coefficient for the medium in question, determines the distance traveled by taking the inverse of the likelihood that an interaction will occur, as seen in **Equation 2** and **Equation 3**.

$$\xi = e^{-\mu x} \qquad (2)$$

$$x = -\frac{1}{\mu} \ln(\xi) \qquad (3)$$

Where μ is the attenuation coefficient of the material, ξ is the random number generated, and x is the distance traveled by the electron.[9] It then checks to see if the calculated distance to interaction occurs within the material used for the calculation within all planes; from the water phantom, this would be the x-, y-, and z-planes. If the particle does interact within the phantom, it moves on to the next step in the process. Suppose it does not fall within the material. In that case, it will terminate the particle or calculate a new distance to interaction within the new medium depending on how the setup is programmed. When an interaction has occurred with a particle, it performs a new random number generation. This number is compared to a probability distribution function determined by the different types of interaction events, E_n, the particle can undergo and defines it between 0 and 1, as seen in **Figure 3**. From the electron beam example,

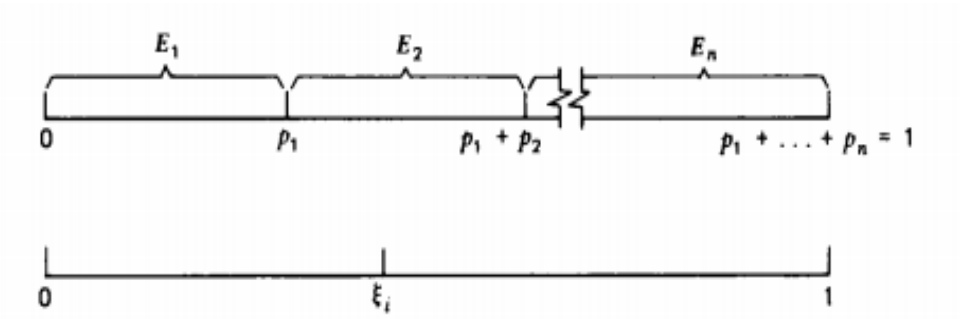

Figure 3. Example of a probability distribution to characterize discrete events and associate an outcome through the use of random number generation between zero and one. Reprinted from "Transport Theory" by James J. Duderstadt and William R. Martin. Copyright 1979 by John Wiley & Sons. Reprinted courtesy of the HathiTrust, under a Creative Commons License https://creativecommons.org/licenses/by/3.0/

there could be an event representing an elastic interaction, inelastic interaction, or a hard collision for three types of events. After determining what interaction type the particle will undergo by using a random number generator, the steps are repeated until the particle is absorbed or leaves the phantom boundaries. This process is repeated for each history or singular particle to provide information regarding how the particle will interact within the medium, how secondary particles come to be and will interact, and how particles are absorbed or terminated within the medium.

2.2.1. TOPAS MC HISTORY

Currently, Monte Carlo methods have been incorporated into many different code types such as MCNP, FLUKA, EGS, and Geant4 as a way for researchers to look at complex systems. Geant4 was an open-source, international project that started in 1994 to improve the Geant3 Fortran code with approximately 100 people working on it.[10] It was developed as a toolkit for simulating particle interactions within matter by tracking particles through different geometrical structures, the nuclear interactions of those particles and materials, and the creations of any secondary particles. It was designed as an object-oriented program with a basis in C++, allowing for anyone to create their code to be utilized within Geant4. This can make Geant4 complicated and tedious for beginners who do not have any coding or Monte Carlo experience.[11]

Tool for Particle Simulation (TOPAS) can be considered a "user code" that is overlayed on to Geant4, which allows for changes and adaptations to be made easily. It was first developed to simplify the currently existing Monte Carlo codes for proton therapy that were too complex for most users. The primary goal was to make proton simulations both reliable and repeatable by simplifying many different aspects of Geant4. It provides the user with the ability to model various complex systems such as linear accelerator gantry heads and x-ray tubes, model dose distributions on CT data provided by DICOM file input, phase space file creation/reading, and more. TOPAS requires the use of simple Text input files, also known as a "User Parameter File," compared to Geant4, which required direct C++ coding. A breakdown of the file format that TOPAS utilizes to run its simulations can be seen in **Figure 4**.[11]

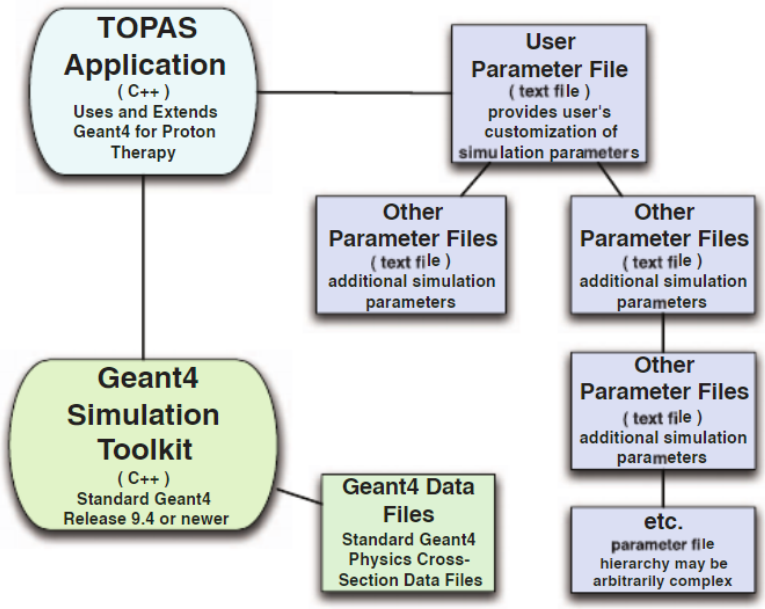

Figure 4. The layout of the TOPAS expansion of the Geant4 toolkit with an example user parameter file and ability to stack parameter files within a file hierarchy system. Reprinted from Medical Physics, Vol 39 Issue 11, H. Paganetti, B. Faddegon, J. Schümann, *et al.*, "TOPAS: An innovative proton Monte Carlo platform for research and clinical applications," 6818 – 6837, Copyright (2012), with permission from John Wiley and Sons.

Each parameter file contains information on geometry, physics, scoring, graphics, particle source, TOPAS control, or time features. The geometry components are made from simplistic models that can be grouped together to form complex shapes and structures. The current version of TOPAS is version 3.6.1, which was released on February 1, 2021. Since the first version of TOPAS was released, the developers have added the ability to model all particle types, made the license easy to acquire for researchers and students by attending a mandatory webinar or paying a licensure fee, and made improvements based on feedback from users.

2.3. AIM OF THE STUDY

This thesis aims to create a functional model of the Elekta Versa HD electron treatment beam utilizing only open-source data that can be used within the Monte Carlo code TOPAS without the need for proprietary information. The model created will be simplistic and annotated to provide ease of access for other users. This work will be passed on to future students to develop

other clinically relevant electron beam energies or be used as a foundation for more computational electron beam research.

3. Methods

3.1. TOPAS MC Simulations

The Monte Carlo code TOPAS was selected as the basis for the Elekta Versa HD linear accelerator model. TOPAS is a simple code designed to remove and minimize errors that were prominent issues with other well-known Monte Carlo codes through the use of engineering controls. Examples of these improvements include removing line-ordering, parameter type specification requirements, introductions of parameter name categories that are mandatory, and requiring no additional external libraries except its foundational code Geant4.

To build a model within TOPAS, the user must specify different physics settings, geometry components, and source information. As an improvement over Geant4, a basic physics list has been created and selected by the TOPAS developers to act as a standardized physics setting. Compared to Geant4, which did not have any form of standardization and could differ between user-to-user based on their preferences or experience. The default physics settings include five modules; for this project, only the "g4em-standard_opt0" module was utilized to focus on the basic electromagnetic physics as only basic geometry components were needed. This physics setting was successfully able to create percent depth dose curves and off-axis profiles for a Varian TrueBeam model at the Rhode Island Hospital/Brown University.[12]

3.2. Electron Beam Simulation

As an electron beam travels along the bending magnet, it is focused on an exit window. It is expected that this beam has a two-dimensional lateral fluence distribution that differs in both direction and energy. It was determined by Loewenthal *et al.* (1992) and Zhu *et al.* (1995) that the fluence distribution of the beam can be modeled with a Gaussian distribution and by Jaffray *et al.* (1993) and Munro *et al.* (1988) that the cross-section maintains an elliptical shape.[13] The

distribution of these factors can slightly differ between different vendors and machines but overall hold the same shape.

Peter Björk, Tommy Knöös, and Per Nilsson (2002) tested how different characteristics of the initial electron beam affect the absorbed dose distribution produced by a linear accelerator by performing Monte Carlo simulations. This paper was the foundation for the settings applied to the initial electron beam within the model created for back iteration. Information provided to them by the manufacturer of the SL25 linear accelerator said that the machine typically has a full width half maximum (FWHM) of 1 millimeter and does not exceed 2 millimeters.[13] These were used as basis numbers for the creation of the outer boundaries of the elliptical shape. This would provide a worst-case scenario and, with limited information, is a safe assumption. The group studied four different geometrical properties for the initial electron beam: a pencil beam, plane-parallel with uniform fluence distribution, plane-parallel with Gaussian fluence distribution, and isotropic point source with a divergent cone angle of 4°. It was determined that any changes to the initial electron beam's geometrical parameters did not affect the relative absorbed dose distribution within the phantom. Changes to the relative absorbed dose distribution and dose profiles were caused by differences in the location and positioning of the components within the gantry head. The recommendation by this group was to put the highest emphasis on the sensitivity of the geometric material within the gantry head, particularly the secondary scattering foil, to make any changes to the lateral dose profiles of the simulation instead of making changes to the initial electron beam characteristics. The final assumption for the initial source beam was that it began after it passed through the exit window. This would create a distance of 100 centimeters between the beginning of the beam and the location of the isocenter.[13]

3.2.1. Gantry Head Geometry

With every major vendor considering component geometry and materials proprietary, information regarding the components within the treatment head is scarce. Time was spent searching through Medical Physics Journals and search engines that access databases of peer-reviewed papers, such as PubMed and NCBI, to find images related to Monte Carlo setups of both electron and photon beams. Articles that included axes with dimensions and locations of components were favored over those that did not have them. This provided a basis for the framework of the treatment head designed for comparison against clinical data. The first paper found utilized a treatment head setup for the Varian Clinac 2100C, a standing-wave linear accelerator with a dual-scattering foil electron system, as seen in **Figure 5**.[14] Through the use

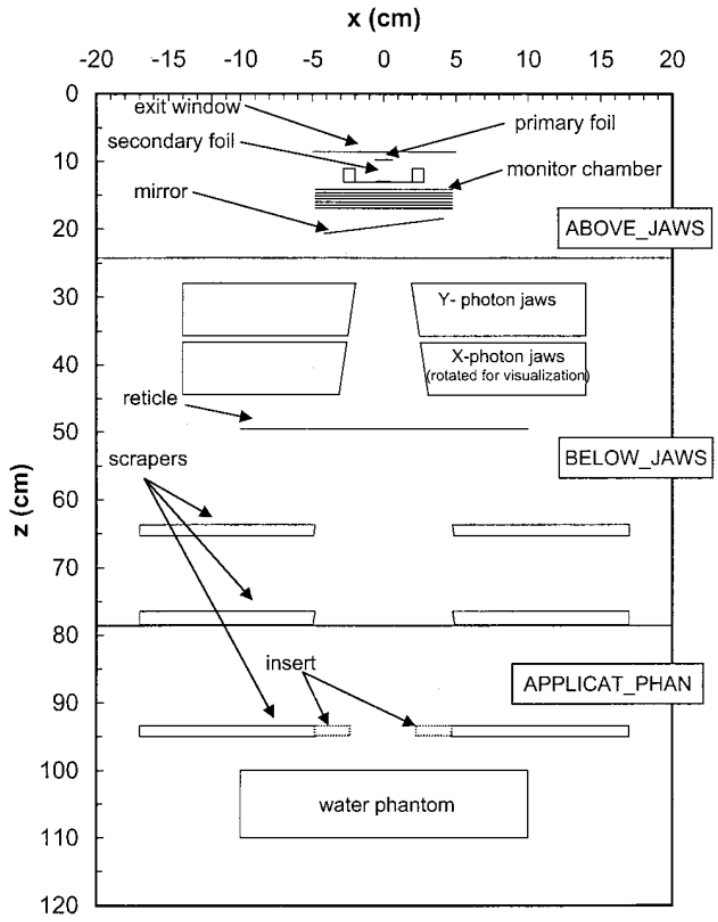

Figure 5. The layout of the BEAM model for the Varian Clinac 2100C linear accelerator used to simulate electron beams. This was used as a basis for determining component sizes and location placement within the TOPAS simulation. Reprinted from Medical Physics, Vol 28 Issue 12, Kenneth R. Hogstrom, John A. Antolak, Michael R. Bieda, "The effect of scattering foil parameters on electron-beam Monte Carlo calculations," 2527 – 2534, Copyright (2011), with permission from John Wiley and Sons.

of a public domain program developed by the National Institutes of Health (NIH) and the Laboratory for Optical and Computational Instrumentation known as ImageJ, distances between two points can be estimated directly from the image. A foundational model was then generated in TOPAS utilizing rough estimates calculated from the image. The components that were focused on included the primary scattering foil, secondary scattering foil, Y-jaws, X-jaws, and the electron cone scrapers. From this paper, the X- and Y-Jaws were modeled within Autodesk® Fusion 360™ (Fusion 360™, Autodesk, San Rafael, California) by forming a right trapezoid in one of the 2-

dimensional planes from the distances measured. The sketch was extruded to have a z-axis length of 25 centimeters as this would be long enough to cover the entire opening of the exit window on the gantry head. The file was exported as a stereolithography (.stl) file and imported into TOPAS by selecting a "TsCAD" geometry type and "stl" file format.

With the clinical data available from an Elekta Versa HD linear accelerator, the Jaw set modeled after a Varian Clinac 2100C is not appropriate for this setting. It worked as a foundational tool for determining flaws within the system and was improved with the finding of papers related to Elekta linear accelerators. These included two Thesis papers by students from Louisiana State University, Guy Merritt Harris (2012) and Justin Deloy LeBlanc (2012), on the Elekta Infinity linear accelerator and an open-source paper by Egor Borzov *et al.* (2017) on the Elekta Versa HD, both of which utilized Monte Carlo simulations.[15–17] From Egor Borzov *et al.* (2017), all major components of interest for the simulation created were shown within the paper, which can be seen in **Figure 6**. Through ImageJ, dimensions were calculated for the "Y- diaphragms" and

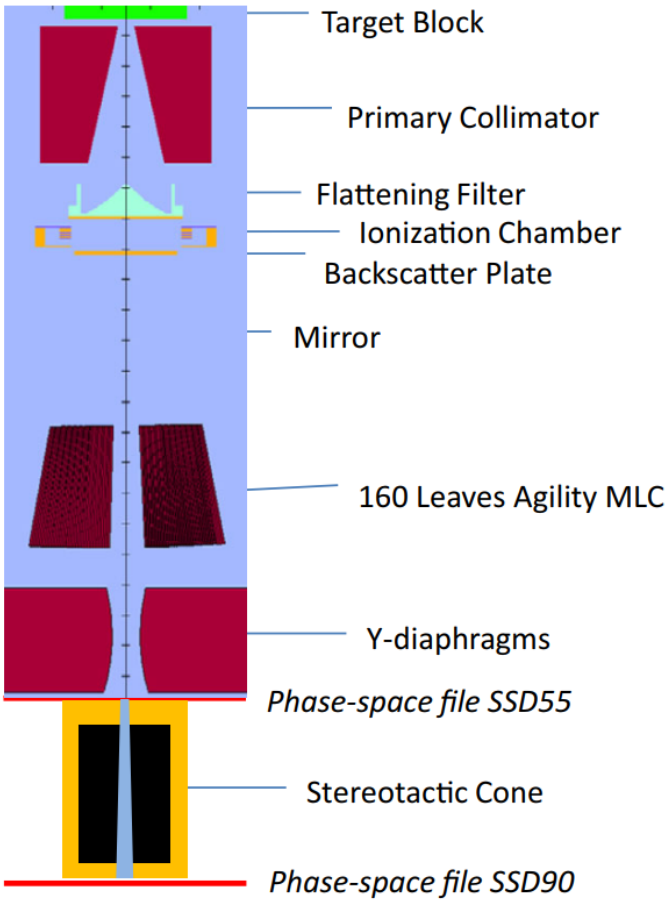

Figure 6. Model of the Elekta Versa HD linear accelerator gantry head developed within BEAMnrc from information provided to the original created through a non-disclosure agreement. Used for the creation of the final model, determining component sizes, and location placement within the TOPAS simulation. Reprinted from "Dosimetric characterization of Elekta stereotactic cones," by Egor Borzov, Alexander Nevelsky, Raquel Bar-Deroma, Itzhak Orion. Copyright (2017) by John Wiley and Sons. Courtesy of the American Association of Physicists in Medicine under a Created Common License CC By 4.0

modeled within TOPAS through a "TsBox" and "G4EllipticalTube" component. In addition to the "Y-Diaphragm," a primary collimator was designed within Autodesk® Fusion 360™ and imported into the simulation to control the direction of the scattered electrons. From **Figure 6**, the distance from the exit window was calculated knowing that the "Phase-space file SSD55" represented a length of 55 centimeters.

3.2.2. Primary Collimator

For the Primary Collimator, dimensions were estimated through the ImageJ process. From **Figure 6**, it was possible to estimate the width and height, x- and z-axes, of the primary collimator. However, due to only having one image, the length of the primary collimator had to be approximated. The primary collimator was designed as a square and extruded to the appropriate height to make it simple. A conical frustum was then removed from the central axis of the primary collimator to act as the guide for the electron beam.

3.2.3. Primary and Secondary Scattering Foils

In the paper by B.J. Patil et al. (2011), the group found that the best materials for the primary scattering foil, based on electron energy loss and bremsstrahlung production, were gold and tantalum. With tantalum being optimized as a primary scattering foil with a thickness of 40 micrometers for a 6 MeV electron beam.[18] As this was a beam modeled created entirely by this group and not related to a clinical system, a thicker primary scattering foil of 60 micrometers was used throughout the project. It is expected that the primary scattering foil holds a circular shape. The diameter was estimated from **Figure 6** and scaled using known machine dimensions. From the geometrical components within TOPAS, the "TsCylinder" geometry type was used in the creation of the primary scattering foil.

As discussed in Section 2.1, the primary scattering foil takes the initial electron pencil beam and creates a Gaussian distribution of electrons. A Gaussian-shaped secondary scattering foil must be used to create a flattened distribution, as seen in **Figure 7**. If only the primary

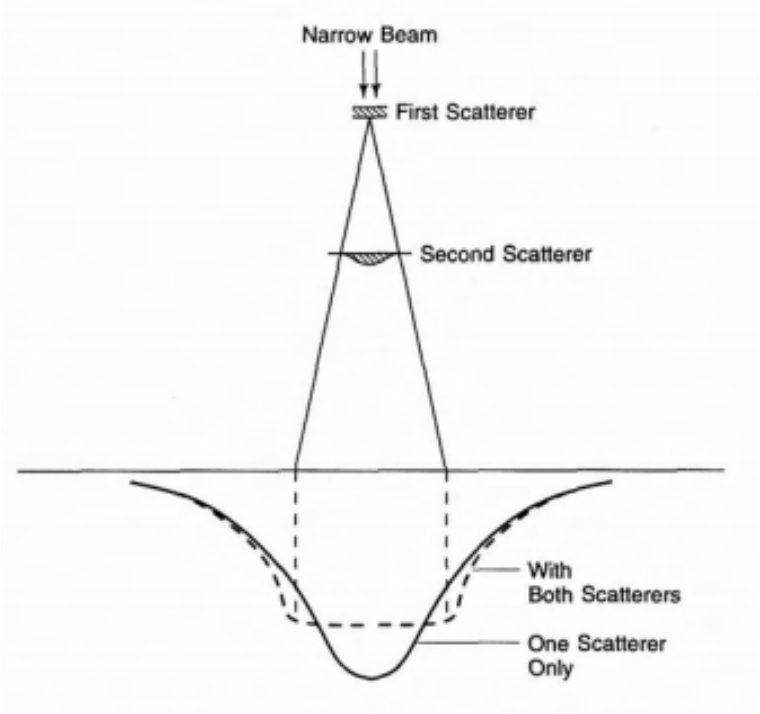

Figure 7. Depiction of how a dual-scattering foil system works to flatten the Gaussian distribution produced by the primary scattering foil. Reprinted from "Medical Electron Accelerators," by C. J. Karzmark, Craig S. Nunan, Eiji Tanabe. Copyright (1991), with permission from McGraw-Hill LLC.

scattering foil is utilized, a forward peaked dose or fluence distribution will be produced. The high-Z material is used for the primary scattering foil to minimize the energy loss of the initial electron beam. A low-Z material is used for the secondary scattering foil, with the thicker portion located along the central axis of the foil to provide greater attenuation.[19] To best simulate the Gaussian shape of the secondary scattering foil, 10 "TsCylinder" geometry components were placed on top of each other in decreasing radii, as seen in **Figure 8**, and were made of Aluminum. An initial

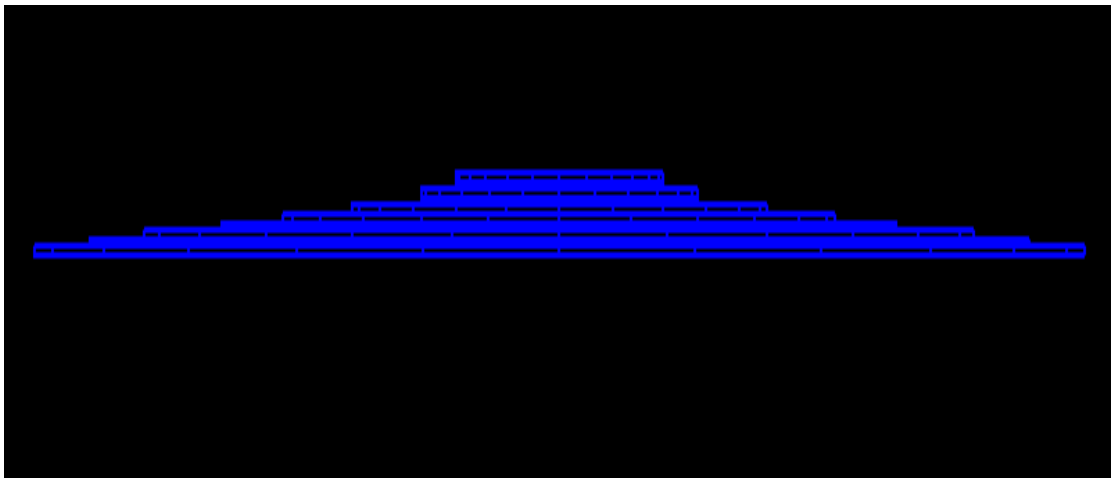

Figure 8. Secondary scattering foil design made of 10 cylindrical disks for a 6 MeV electron beam.

thickness of 0.5 centimeters was selected based on the optimum dimensions of the primary and secondary scattering foil from the paper by B.J. Patil *et al.* (2011).[18] The secondary scattering foil is the primary component that finding information for was challenging to locate due to its unique shape and dependence on the primary scattering foil; this led to the need for an iterative process to determine the appropriate thickness. A flowchart of the approach taken can be found in Appendix 8.1. A ring or holder was created around the foil to represent the carousel system to imitate the secondary scattering foil setup utilized within modern linear accelerators. It was assumed that this component was made of a mild steel alloy consisting of eight different elements and a density of 7.85 grams per cubic centimeter. The breakdown of the material composition was created so that the elemental weight fractions summed to one and is shown in **Table 1**.

Table 1. The atomic weight fractions used in the formation of a mild steel material within TOPAS.

Element	Weight Fraction [%]
Aluminum	0.0230
Carbon	0.2950
Chromium	0.0240
Copper	0.0320
Manganese	0.4110
Nickel	0.0290
Silicon	0.1711
Sulfur	0.0149

3.2.4. Electron Cone Applicators

The electron cones were modeled utilizing measurements physically acquired from the Elekta Versa HD electron cones. This was performed on all clinically used electron cones: the 6x6, 10x10, 14x14, 20x20, and 25x25 cm^2 field size cones. The axes of the electron cones were split into long and short axes, as seen in **Figure 2**, which served as a basis for the modeling through "TsBox" components within TOPAS. To ensure that the component was not a slab of solid material, a "daughter" of each applicator slab was created inside it. The "daughter" component was made of air and extended through the entire slab to properly simulate any openings.

Assumptions on the physical characteristic of the scrapers were based on the Thesis paper by Marie-Louise Olsson (2003), a Lund University Hospital graduate from Lund, Sweden, Monte Carlo simulations were performed to determine the characteristics of electron applicators for an Elekta SLi Plus linear accelerator. This type of linear accelerator utilized electron cone applicators with open sides similar to those for the Versa HD. The scrapers in this paper are a combination of lead and aluminum plates in rotating order, as seen in **Figure 9**.[20] This served as an explanation

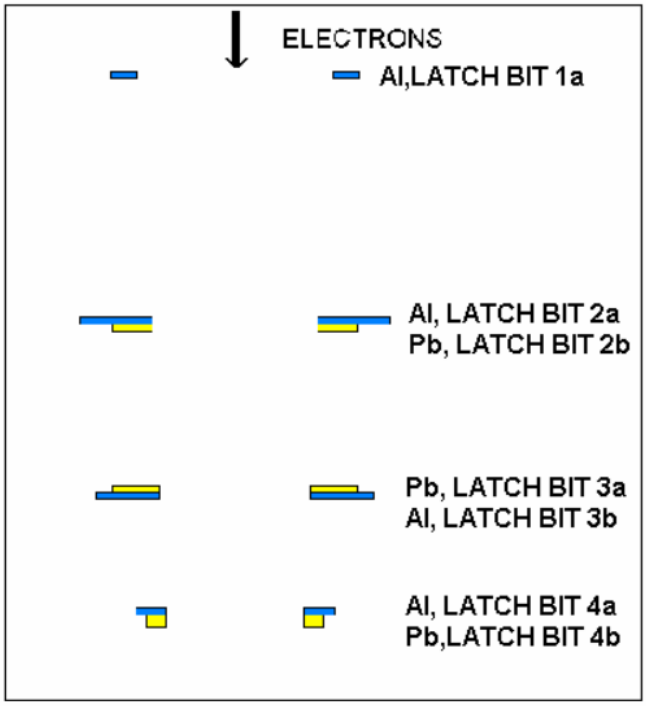

Figure 9. Electron Cone applicator layout for an Elekta SLi Plus linear accelerator built within the Monte Carlo code BEAMnrc. Reprinted from "Monte Carlo simulations of the Elekta SLi Plus electron applicator system – A base for a new applicator design to reduce radiation leakage," by Marie-Louise Olsson (Now: Dr. Marie-Louise Aurumskjöld) (2003) with permission from Author.

for the material of the electron cone's scrapers, which are represented by each "LATCH BIT" that were used for the iterative modeling of an electron beam.[20] Each scrapper could be made of a Zinc alloy, such as the electron cone for the Varian Clinac 2100C. However, without any knowledge of the mass percent of each element within the alloy, it is practically impossible to model this correctly.

3.2.5. Data Acquisition Through Scoring

When measuring dose or output from a linear accelerator, the most accurate measurements are taken with an ionization chamber placed in a water phantom. This is based on Report Number 67 from Task Group 51 on the protocols for clinical reference dosimetry. With Monte Carlo techniques, it is possible to model measurements directly from the water phantom

without the need for a measurement device such as an ionization chamber. The water phantom was placed 100 centimeters away from the exit window and measured 40 by 40 by 40 cubic centimeters. TOPAS offers various quantities that can be scored, such as dose to water, dose to a medium, energy deposited, and fluence. For this project, the absorbed dose to water was calculated through the phantom by creating bins. The number of bins selected for this phantom can be seen in **Table 2,** with the orientation of the phantom illustrated in **Figure 10**. Each bin

Table 2. Bin numbers used in the water phantom for scoring of dose deposition.

Axis	Number of Bins
X	800
Y	800
Z	1

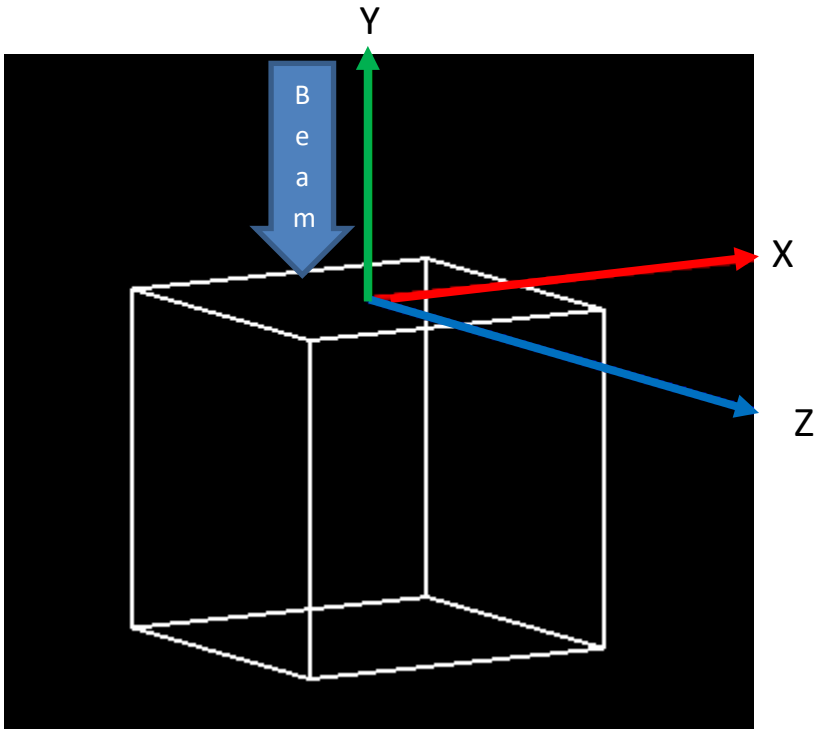

Figure 10. Water Phantom projection showing the axes and orientation of the incident beam.

would have an output value that could be used to determine the dose to water at a set depth and position within the water phantom.

3.2.6. Iteration & the Graphical User Interface

TOPAS allows for different data output types during scoring, such as root, binary, DICOM, XML, and CSV, which can be used in the analysis process.[11] This data needed to be compared to other datasets in a readily accessible, simplistic, and efficient setting. A Graphical User Interface (GUI) was created to enable the user to accomplish these goals. The GUI offers the user the ability to develop an off-axis profile from the data acquired in a CSV file format through the TOPAS scoring system, select the appropriate electron cone size that was used for the simulation, and whether or not the user would like to compare the data to that from the clinical setting. This data was acquired using a synthetic PTW microDiamond detector (Type 60019, PTW-Freiburg, Freiburg, Germany) measured at a source-to-skin distance of 100 cm, with one using the 10 cm^2 electron cone and another using the 14 cm^2 electron cones. An example of the format is shown in **Figure 11**. The GUI also allows the generation of a Percent Depth Dose (PDD) curve **Figure 12**,

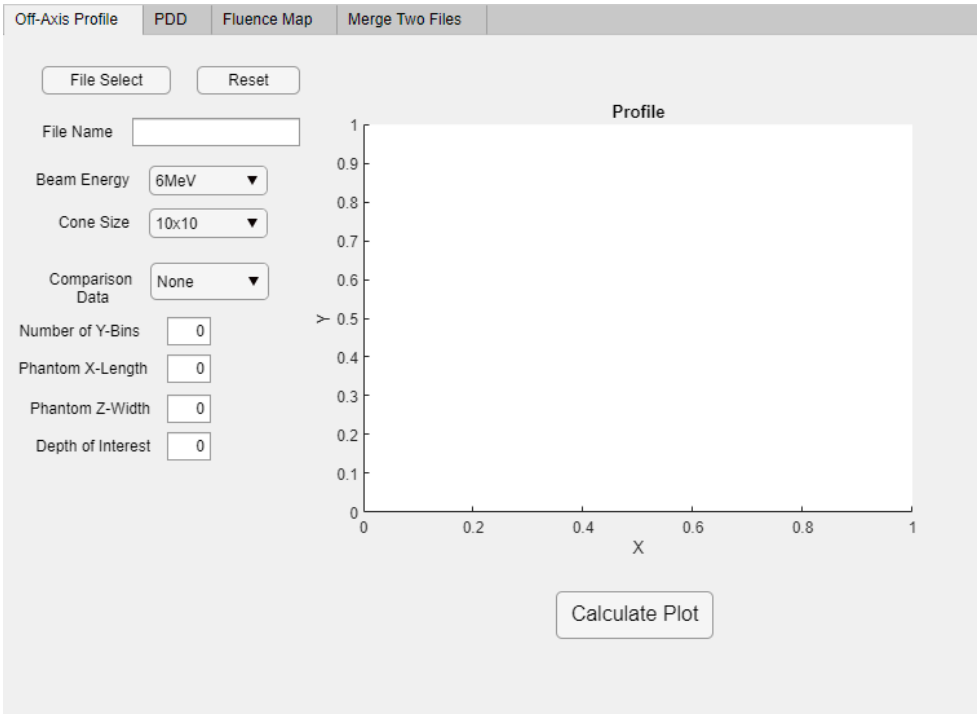

Figure 11. A screenshot of the off-axis profile tab within the graphical user interface.

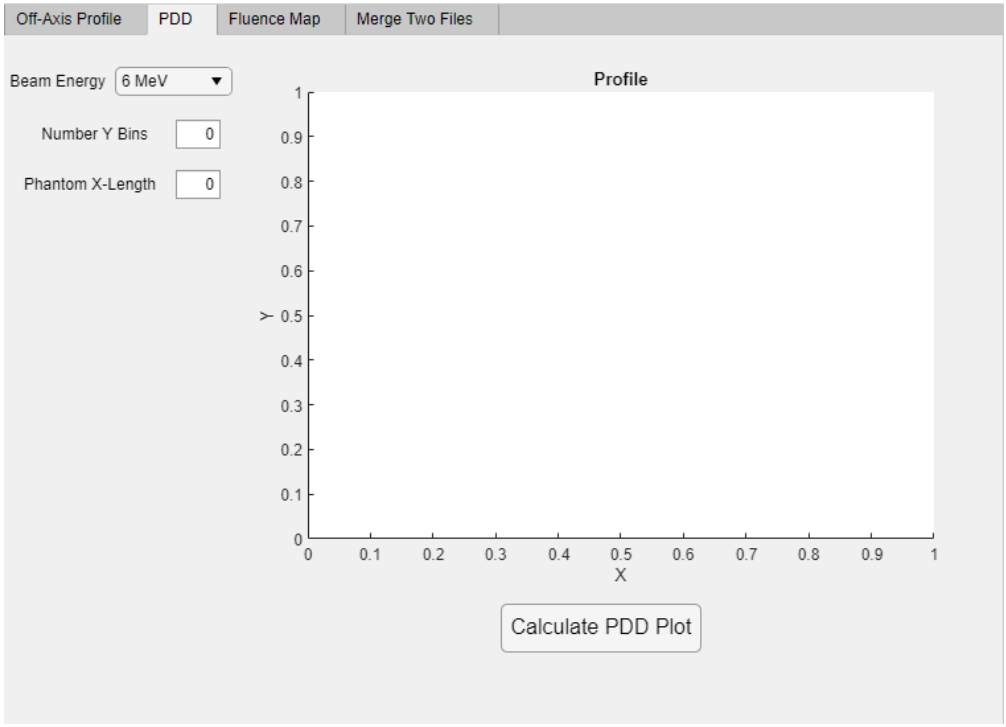

Figure 12. A screenshot of the percent depth dose profile tab within the graphical user interface.

fluence map generation and the ability to add the dose or fluence values from two different CSV files to create one merged file. The section of the GUI that produces fluence heat maps was developed to work for a single plane, 2-dimensional, surface fluence scoring. An example of an appropriate scoring plane would be to look at the surface of an 800 by 800 by 1 scoring component. The darker the location within the heat map, the larger the number of particles that traveled through the bin. The user can use these tools to get an idea of how the simulation is trending towards matching the available clinical data. The GUI is a small part of determining the appropriate size of the secondary scattering foil. An iterative process was used by selecting a new secondary scattering foil thickness, have the simulation run utilizing a history count of 100 million, and then analyzing the data through the GUI to determine if the following thickness should be higher or lower. This process was repeated until the appropriate off-axis profile, and PDD curve was created.

As TOPAS and other Monte Carlo codes utilize the central processing unit (CPU) threads to simulate each history, it is time-consuming. The larger the number of threads within the CPU, the faster the simulation will run. This project was initially started on a laptop with a four threads Intel® Core™ i7 dual-core processor that could complete a 100 million history simulation in approximately 15 to 17 hours. This project was slowly worked on between August and December of 2020 before upgrading to an AMD Ryzen 9 12-Core processor with 24 threads. The upgrade allowed for a simulation of 100 million histories to be completed within 3 to 4 hours. This was used to complete the final model of the system and went through approximately 30 versions.

4. Results

4.1. Modeled Components

4.1.1. Component Placement

It is important not only to understand the size of each component and how the physics related to each component works but also the placement of each component within the system. A formal understanding of talking about distance is source-to-skin distances (SSD), which was utilized here. The distances from the source, or exit window, to the top of each component were measured through the use of **Figure 6** and can be found in **Table 3**.

Table 3. The distance from the exit window of the simulation to the top of each component that was modeled within the system.

Component	Distance from Exit Window to Top of Component [cm]
Primary Scattering Foil	1.997
Primary Collimator	2.100
Secondary Scattering Foil Holder	13.000
Secondary Scattering Foil	14.745
MLCs	33.330
Y-Diaphragms	46.140
Gantry Head Plate	54.500
Electron Cone	55.000
Water Phantom	100.000

4.1.2. Primary Collimator

A square, rectangular prism was created with a conical frustum removed from the central axis, as discussed earlier. The dimensions of the component can be seen in **Table 4**. The primary

Table 4. Dimensions calculated for the creation of the primary collimator.

Side	Length (cm)
Length [X]	35
Width [Y]	35
Height [Z]	9.8
Frustum Base Diameter	5.077
Frustum Top Diameter	1.9

collimator was given a material compound of Tungsten, and a section analysis of the component can be seen in **Figure 13**.

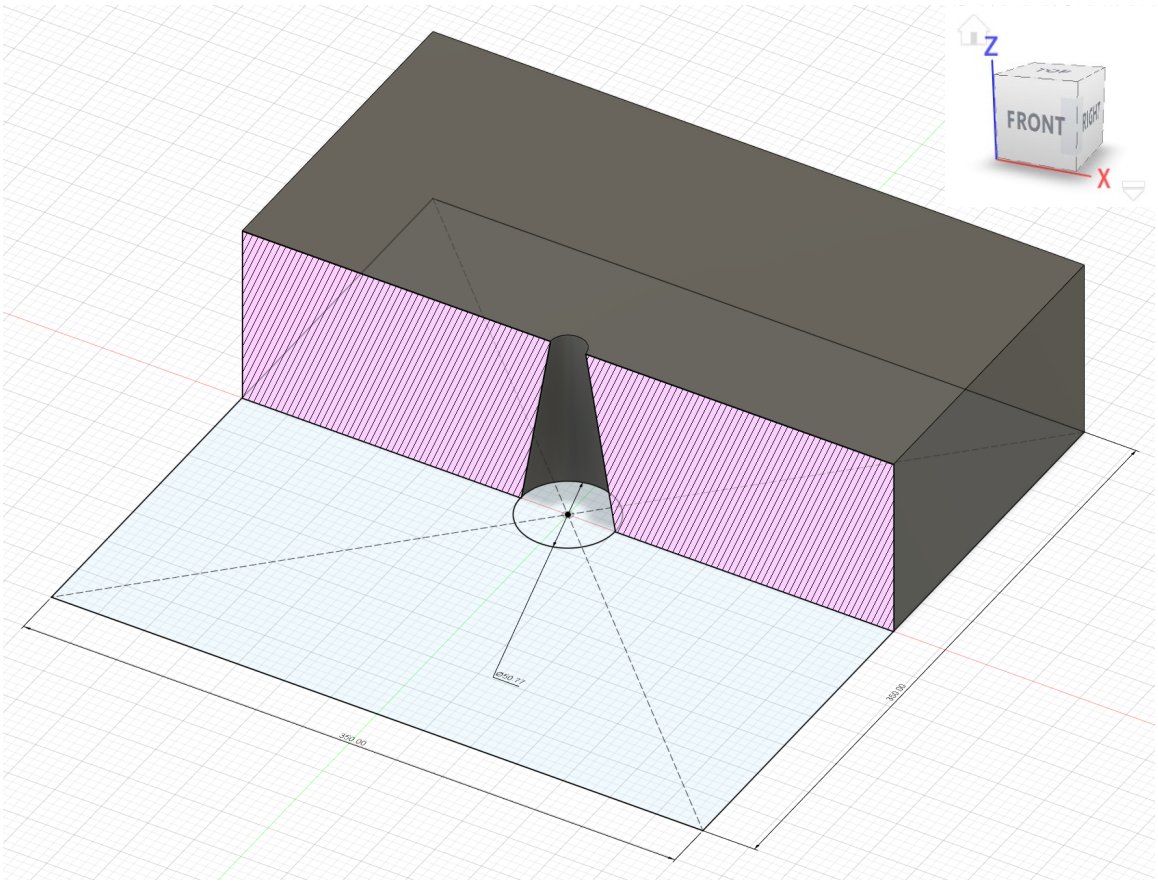

Figure 13. A screenshot of a section analysis of the primary collimator created within Autodesk® Fusion 360™.

4.1.3. MLC and Jaws

The MLC and Jaw systems were modeled utilizing the same components for each, and two models were created based on **Figure 5** and **Figure 6**. Just as with the primary collimator, the width of the components could not be determined as there was only one image depicting two

axes. Dimensions of the modeled component based on the Varian Clinac 2100C from **Figure 5** can be seen in **Table 5**. This design was later changed to match information on the Elekta Versa HD.

Table 5. The dimensions calculated through ImageJ from the Varian Clinac 2100C used in the creation of the MLC/Y-Diaphragm components.

Side	Length [cm]
Top	12.0
Vertical Line – Left Side	7.50
Bottom	11.0

The final Jaw/MLC component information was estimated from **Figure 6** and can be seen in **Table 6**. As stated earlier in the paper, this component was created within TOPAS through the simple

Table 6. The dimensions calculated through ImageJ from the Elekta Versa HD used in the creation of the MLC/Y-Diaphragm components.

Side	Length [cm]
Length of Rectangular Prism [X]	15
Width of Rectangular Prism [Y]	25
Height & Ellipse Major Axis [Z]	8.306
Ellipse Minor Axis	1.282

geometry components within the TOPAS software. However, a model was rendered within Autodesk® Fusion 360™ to create a clearer representation of the component, which can be seen in **Figure 14**.

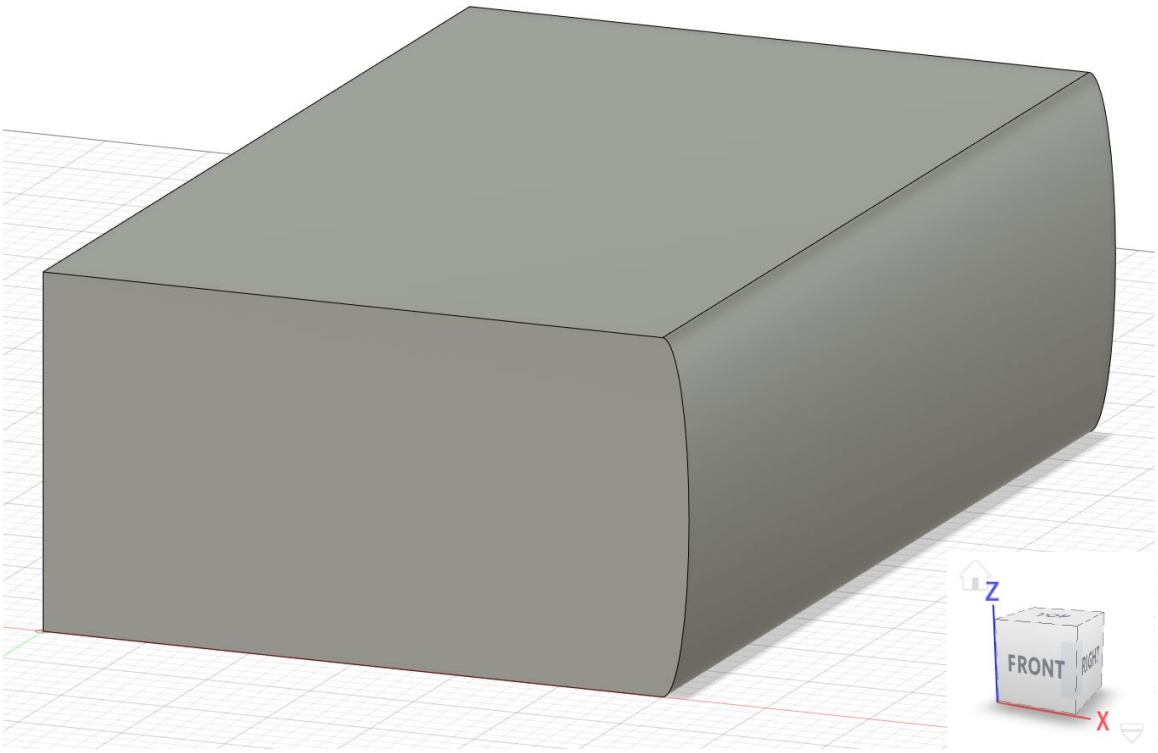

Figure 14. A screenshot of the multi-leaf collimator block and Y-diaphragm created within Autodesk® Fusion 360™.

4.1.4. Electron Cones

Each electron cone was measured for a model to be created within TOPAS. Utilizing the axis system shown in **Figure 2** and numbering system used in the thesis by Marie-Louise Olsson (2003), the dimensions of each electron cone scraper and the height between each level can be found in **Table 7** and **Table 8**.[20] Two versions of the electron cones were created, one was created

Table 7. Dimensions of each scraper measured from the Elekta Versa HD electron cones used in the clinic.

Scraper	Axis	06 Cone [cm]	10 Cone [cm]	14 Cone [cm]	20 Cone [cm]	25 Cone [cm]
Base (1a)	Across – Open	10.0	14.2	16.0	18.0	21.0
	Across - Total	18.2	18.1	24.0	24.0	25.0
	Long – Open	10.0	14.2	16.0	18.0	19.0
	Long - Total	29.0	28.0	29.0	29.0	31.0
Scraper (2a)	Across – Open	9.4	13.0	16.0	20.0	24.0
	Across - Total	20.8	23.8	26.8	30.8	33.0
	Long – Open	9.4	13.0	16.0	20.0	24.0
	Long - Total	21.0	23.8	26.8	30.8	33.0
Scraper (2b)	Across – Open	9.4	13.0	16.0	20.0	24.0
	Across - Total	20.8	22.0	25.0	29.0	33.0
	Long – Open	9.4	13.0	16.0	20.0	24.0
	Long - Total	21.0	22.0	25.0	29.0	33.0
Scraper (3a)	Across – Open	7.1	11.0	14.0	20.0	25.0
	Across - Total	14.6	18.4	21.4	27.6	32.0
	Long – Open	7.1	11.0	14.0	20.0	25.0
	Long - Total	14.4	20.4	24.8	28.6	32.2
Scraper (3b)	Across – Open	7.1	11.0	14.0	20.0	25.0
	Across - Total	14.2	18.0	20.8	26.1	32.0
	Long – Open	7.1	11.0	14.0	20.0	25.0
	Long - Total	14.2	18.0	21.0	26.9	32.0
Scraper (4a)	Across – Open	6.0	10.0	14.0	20.0	25.0
	Across - Total	9.5	13.0	17.4	23.4	28.5
	Long – Open	6.0	10.0	14.0	20.0	25.0
	Long - Total	10.3	14.5	18.4	24.0	29.2
Insert (4b)	Across – Open	6.0	10.0	14.0	20.0	25.0
	Across - Total	9.0	12.0	17.0	23.0	28.0
	Long – Open	6.0	10.0	14.0	20.0	25.0
	Long - Total	9.0	12.0	17.0	23.0	28.0
	Thickness	1.0	1.0	1.0	1.0	1.0

Table 8. Distance between each scraper set measured from the Elekta Versa HD electron cones used in the clinic.

	Distance [cm]				
Scrapers	**06 Cone**	**10 Cone**	**14 Cone**	**20 Cone**	**25 Cone**
1a to 2a	21.0	17.1	17.0	17.0	17.0
2b to 3a	7.8	11.5	11.5	11.6	11.5
3b to 4a	7.3	7.2	7.3	7.0	7.3

within Autodesk® Fusion 360™ and assigned as entirely Tungsten, while the second was made from basic geometry components within TOPAS. The two different versions can be seen in **Figure 15** and **Figure 16**.

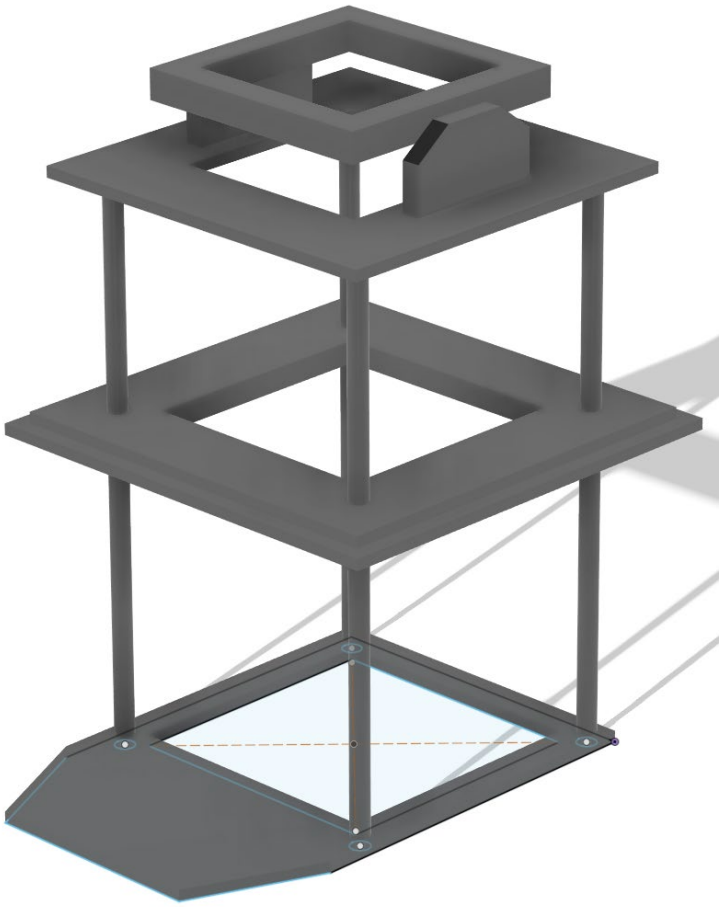

Figure 15. A screenshot of the 10 by 10 cm^2 field size electron cone created within Autodesk® Fusion 360™.

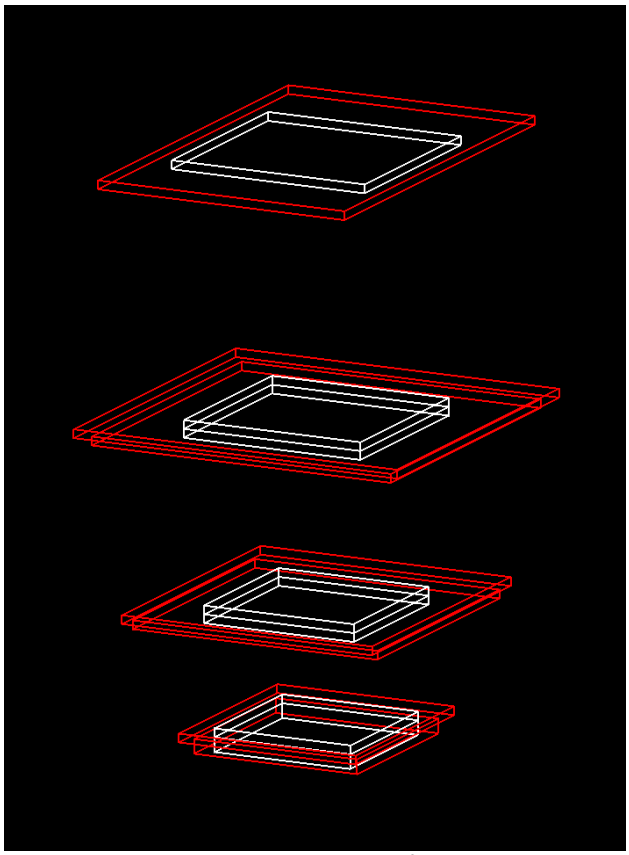

Figure 16. A screenshot of the 10 by 10 cm^2 electron cone system created within TOPAS using basic geometry components.

4.1.5. Secondary Scattering Foil

The secondary scattering foil required time and an iterative process of looking at off-axis profiles and PDD curves. The aluminum secondary scattering foil went through countless designs utilizing different central axis thicknesses. The total sum differences between data obtained from the simulation and clinical data for sections of the off-axis profiles were used during the iterative process to help determine the following thickness. Bar graphs showing the differences for each section of the last four simulations can be seen in **Figure 17**. Larger versions of each plot can be

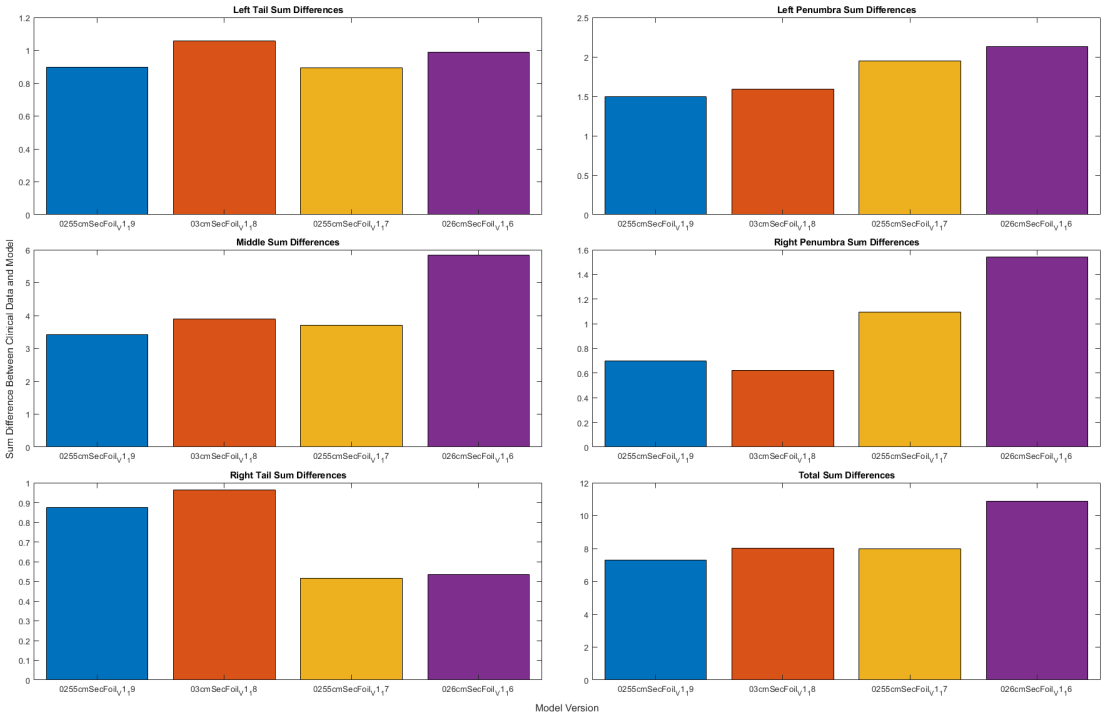

Figure 17. The total sum difference between each point of the simulation data and the clinical data within different locations of the off-axis profile for the 6 MeV energy electron beam at a depth of 1.4 cm and 10 by 10 cm^2 field size. The blue bar is data from version 1.19 with a 0.255 cm secondary scattering foil thickness, and the red bar is from version 1.18 with a 0.3 cm secondary scattering foil which both use the TOPAS built electron cone. The yellow bar is data from version 1.17 with a 0.255 cm secondary scattering foil, and the purple bar is version 1.16 with a 0.26 secondary scattering foil thickness which both use the imported electron cone.

found in the Appendix 8.2. It was determined that a foil thickness of 0.255 centimeters produces both an off-axis profile and PDD curve comparable to clinical data, which can be seen in **Figure 18**

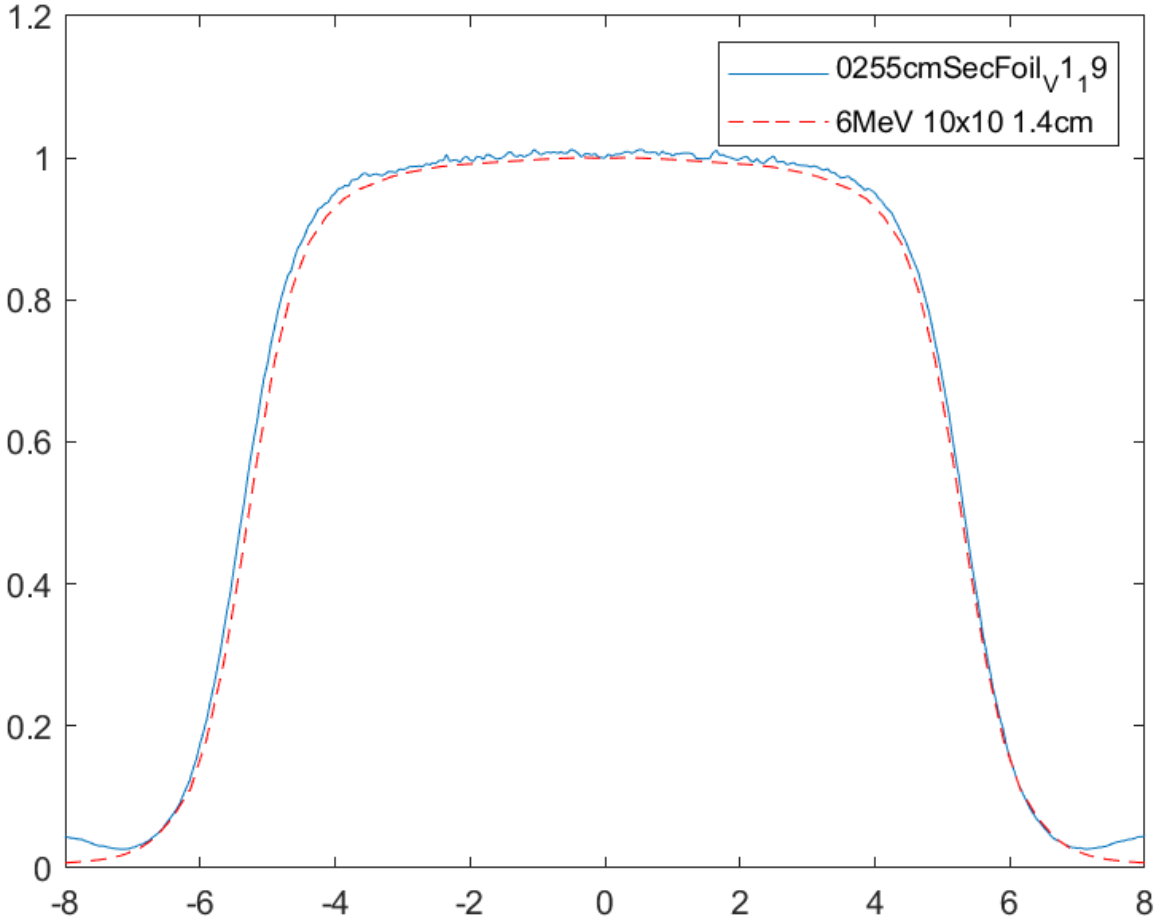

Figure 18. The off-axis profile for comparison of the 2 billion history count simulation for the final version of the model, which uses a 0.255-centimeter secondary scattering foil thickness, for a 10 by 10 cm^2 field size versus the clinical data at a depth of 1.4 centimeters.

and **Figure 19**. For the percent depth dose curve, different clinically relevant points were

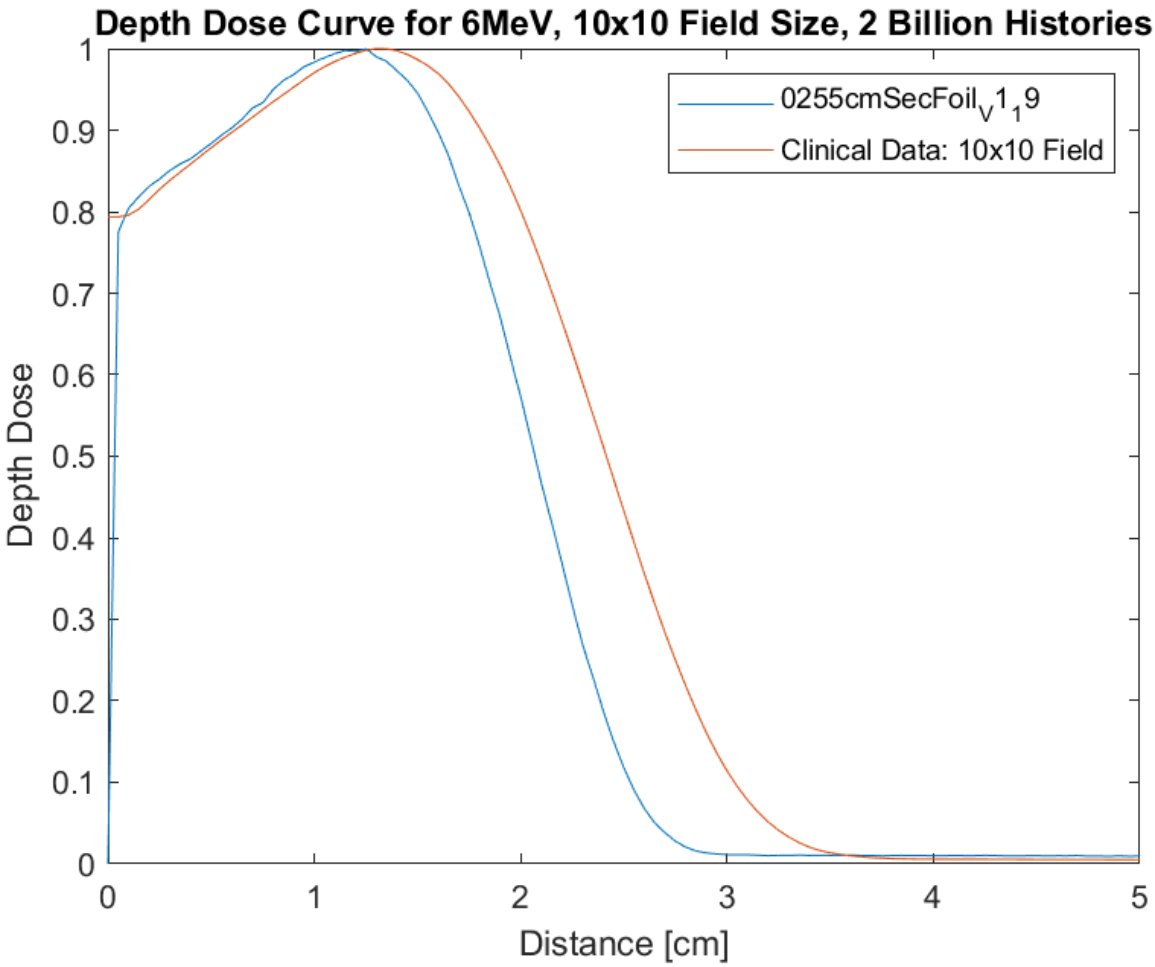

Figure 19. The percent depth dose curve for comparison of the 2 billion history count simulation for the final version of the model, which uses a 0.255-centimeter secondary scattering foil thickness for a 10 by 10 cm^2 field size versus the clinical measured data.

compared to determine agreement between the two curves and can be seen in **Table 9.** From

Table 9. Data point comparison between simulation data and measured clinical data.

	Measured Data	**Simulation Data**	**Percent Difference [%]**
Surface Depth Dose	0.7937	0.7754	2.306
D_{max}	1.300 cm	1.250 cm	3.846
R_{90}	1.806 cm	1.140 cm	36.88
R_{80}	2.001 cm	1.450 cm	27.54
R_{50}	2.415 cm	2.069 cm	14.33

the off-axis profile, the full width at half maximum (FWHM), locations of the penumbras, and flatness for the clinical measured data and simulation data were compared and shown in **Table 10**.

Table 10. Data point comparison between simulation data and measured clinical data.

	Measured Data	**Simulation Data**	**Percent Difference [%]**
Flatness	3.027%	3.134%	3.41
FWHM	10.556 cm	10.694 cm	1.29
Left Tail: -8.15 cm	0.00655	0.0471	86.1%
Right Tail: 8.2 cm	0.00631	0.0463	86.4%
	Measured Data	**Simulation Data**	**Distance-to-Agreement [cm]**
Left Penumbra 20% - Start	-5.859 cm	-5.927 cm	-0.068
Left Penumbra 80% - End	-4.678 cm	-4.804 cm	-0.126
Left Penumbra Width	1.181 cm	1.123 cm	N/A
Right Penumbra 80% - Start	4.678 cm	4.749 cm	0.071
Right Penumbra 20% - End	5.859 cm	5.889 cm	0.030
Right Penumbra Width	1.181 cm	1.140 cm	N/A

4.2. Final Model

All components were placed within the model, and the secondary scattering foil thickness was adjusted to produce off-axis profiles and PDD curves that were comparable to clinical data. As stated before, the final model consisted of a primary scattering foil, primary collimator, secondary scattering foil and holder, multi-leaf collimator blocks, Y-diaphragm blocks, gantry head faceplate, gantry shielding cover, electron cone applicator system, and the water phantom. These components, except for the gantry shielding cover, can be seen in **Figure 20** and **Figure 21**.

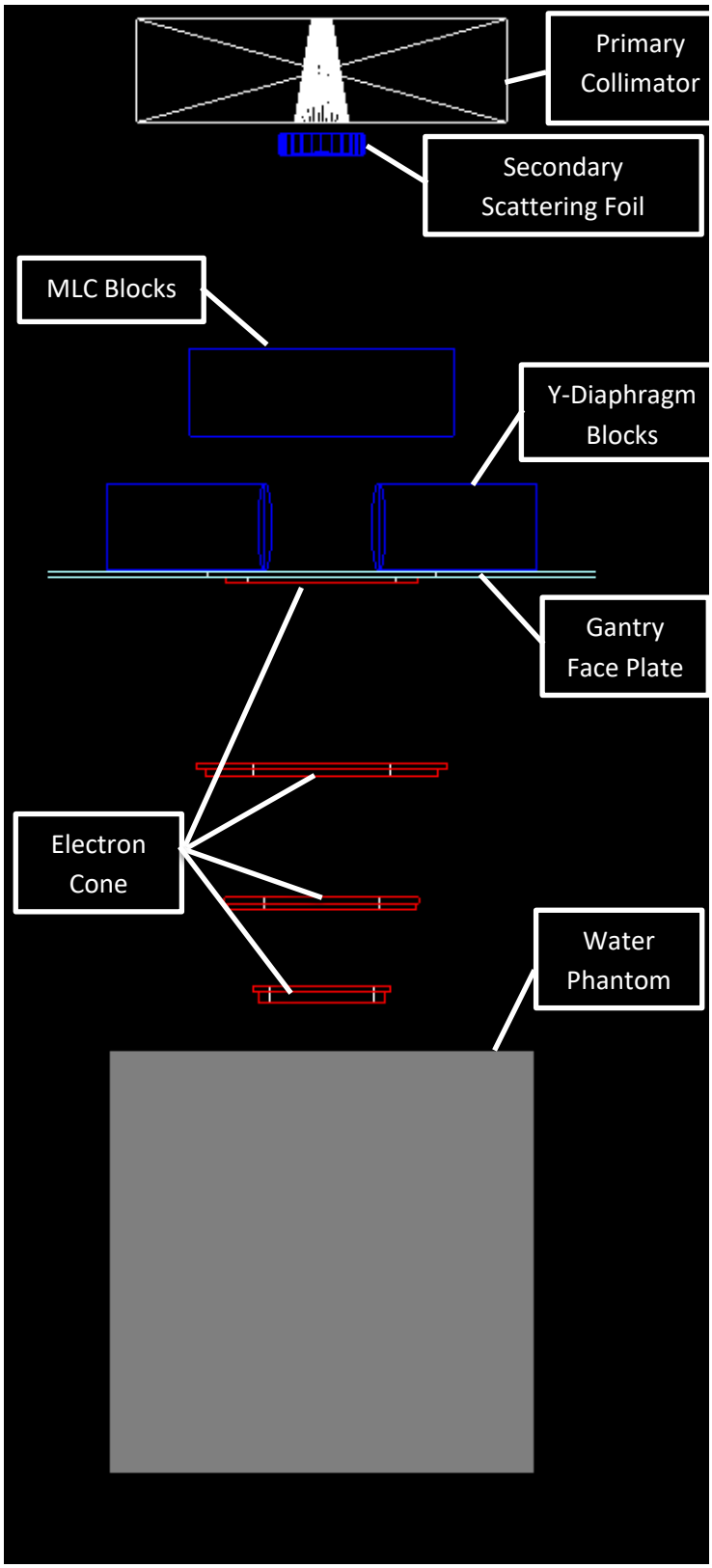

Figure 20. A screenshot of the final electron beam model minus the gantry shielding cover is shown in the graphical display settings within TOPAS.

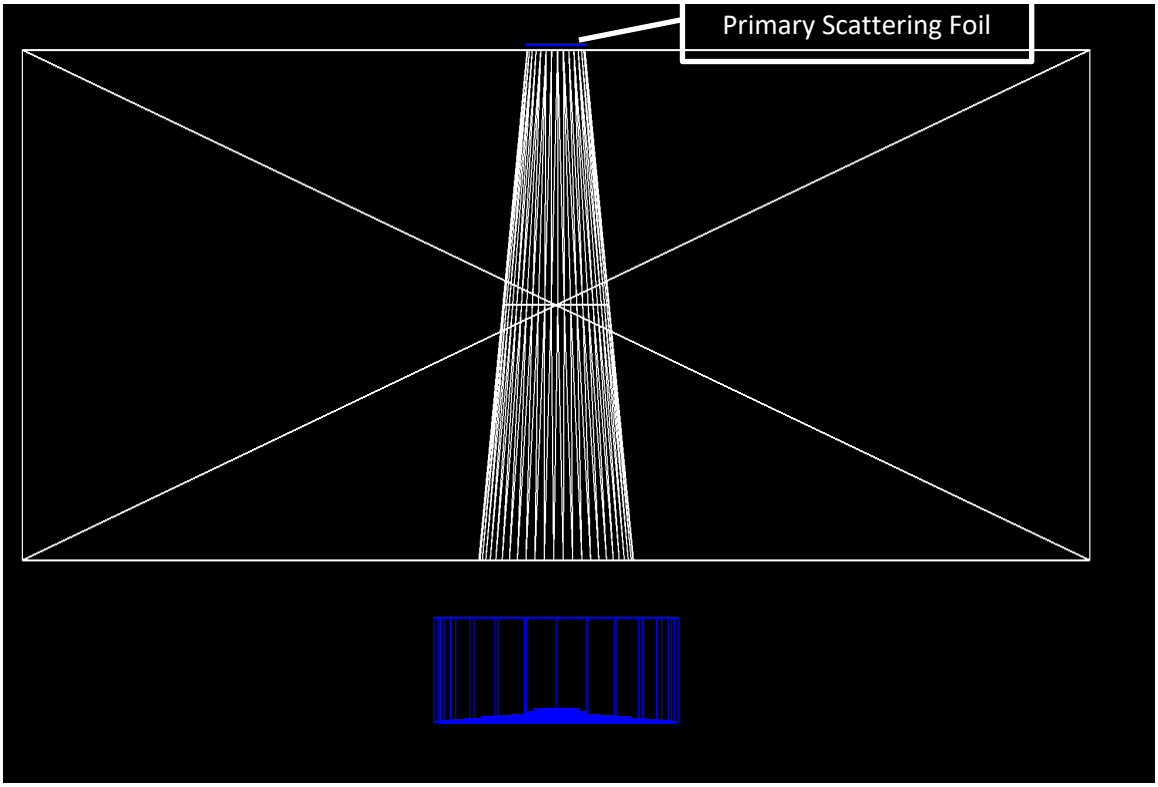

Figure 21. A zoomed-in shot of the final electron beam model to showcase the small primary scattering foil located above the primary collimator.

5. Discussion

5.1. Complete Model

As seen in **Figure 18**, the data for the 0.255-centimeter scattering foil produces comparable data to clinical data. It should be noted that the clinical data that was used was acquired from quality assurance data. This means that the data had been post-processed by a viewing/acquisition software, such as PTW's MEPHYSTO software. During post-processing, the software adjusts the data by smoothing the raw data to remove noise and mirroring to create flat profiles. The data acquired from the TOPAS simulation is raw data; it is best represented by non-processed, off-axis profile data obtained through the use of a water tank setup. For the sake of this project, the processed data is appropriate in the iterative process to narrow down a model that was comparable to a clinical system. The penumbral region of the simulation data follows approximately the same slope. The left penumbral region differs between the clinical measured data and the simulation data by 5.17%, and the right penumbra differs by 3.60%. The FWHM between the two data sets differs by 1.29% or 0.138 cm, with a flatness difference of 3.41%. The simulation data does, however, have a longer flattened region when compared to the clinical data. The clinical data has a lower intensity along where the edge of the applicator system would be, which could be caused by the data being post-processed or volume averaging within the detector used to measure the clinical data. Compared to the simulation, in which each bin is separate and does not have any volume averaging caused by a traveling detector. The percent depth dose curve, **Figure 19**, created utilizing the 0.255-centimeter field size, has a faster dose falloff than the acquired clinical data. The steeper slope of the curve is potentially due to similar volume averaging issues experienced in the penumbral region of the off-axis profile. However, the difference between the two plots is most likely caused by attenuation of the beam within the secondary scattering foil that causes the beam energy to be lower than expected. The shape of

the percent depth dose curve is closer to a 5 MeV electron beam when comparing the different location points. For example, R_{80} for the simulation data is 1.450 cm, and for a 5 MeV electron beam, it is expected to be approximately 1.660 cm.

Compared to other versions, **Figure 17**, the middle and left penumbral sections produced the lowest difference between the clinical data and the 0.255-centimeter scattering foil. However, the tail differences were exceptionally high, having the largest percent difference of 86.1% on the left tail and 86.4% on the right tail, after introducing the basic geometry components compared to the 3D rendered components, which will be discussed later. The version that used the 3D rendered electron cone and a 0.255-centimeter scattering foil thickness still produced the lowest difference between the simulation and clinical data.

5.2. Model Limitations

Most of the acquired data during this process utilized only 100 million counts, which, with a computer that contained a 12-core, 24 thread, processor would take approximately 3 to 4 hours to compute. Unfortunately, when a low number of histories are used within the simulation, it increases the noise of the plot. An example of this can be seen in **Figure 21** in Appendix 8.2, where the data is inconsistent and jagged. More extended simulations could be done to minimize the noise within the plots, such as in **Figure 18**, but could take up to 50 hours to achieve history counts of 2 billion. With the appropriate setup, such as access to a supercomputer or cluster with higher thread counts, faster and more extensive data acquisition would be possible. With only access to the computer mentioned earlier, this limiting factor made it possible to run through one or two simulations per day for data acquisition at history counts of 100 million.

At one point in the model creation process, the multi-leaf collimators and “Y-Diaphragms” were put into the model by importing stereolithography files. This put a total of six components

within the model that was imported from Autodesk® Fusion 360™. The components were the primary collimator, the multi-leaf collimator blocks, the “Y-Diaphragm” blocks, and the electron cone applicator. Simulations started to throw an error or exception, which stated particles were stuck or not moving and caused a particle termination. If enough particle terminations occur due to the exception, the entire simulation will terminate due to code built-in to TOPAS. Using the TOPAS user forum, users found that the resolution of the exported stereolithography files plays a significant role in the exception error occurring. Lower resolutions result in fewer areas in which particles can get stuck. One issue with lowering the resolution of the exported component is a loss in the accuracy of the component's dimensions. In all, this limits the user's ability to create an entire model through 3D rendered objects.

5.3. Future Work

It would be possible to use this process to expand to other clinically relevant electron energies such as 8, 10, 12, and 15 MeV electron beams. From the experience of this paper, it would be best to do this on either multiple computers, each running a separate simulation with a different secondary scattering foil thickness, or invest in access to a supercomputer with a large number of threads. This would allow for faster simulations and larger history counts to be run-producing data with lower noise contamination within the plots. It would also be beneficial for a future project to fix the issue with the large difference between the percent depth dose curve of the simulation and clinical measured data. This could be accomplished by increasing the energy of the initial beam and repeating the iteration process, such as in **Figure 30** in Appendix 8.2.

An influx of contamination radiation occurred outside the penumbral region during the transition between electron cone applicator models. It is expected that the most considerable radiation contamination would only produce intensities of 2 or 3% within the percent depth dose

curve, which could be caused by radiation that passes through the opening of the electron cone or is produced as a secondary reaction from an interaction of the electrons with the material of the cone.[21] From the off-axis profiles, **Figure 22** and **Figure 23**, approximately two to three centimeters outside of the penumbral region intensity, increases between 0.05 and 0.08 can be seen. This is unlike the Autodesk® Fusion 360™ applicator system, which follows the clinical data and decreases to approximately zero. Future work should be done to determine the cause of the contamination radiation within the off-axis profile and beam model.

5.4. Conclusion

This study shows that it is possible to create an electron beam model through an iterative process by comparing acquired data to clinical data from an Elekta Versa HD linear accelerator. It was determined that for a 6 MeV electron beam, a secondary scattering aluminum foil thickness of 0.255 centimeters produced data that was comparable to the clinical data within the off-axis profile. However, this was an estimate through the use of ten cylindrical stacked disks to represent the Gaussian shape used within clinical linear accelerators. Each of the other components could be modeled through the use of 3D modeling software or basic geometry components built-in to the TOPAS software. Component information was available throughout the literature; however, most images were rough approximations and did not provide absolute data. In conclusion, this study has shown that the 0.255 cm secondary scattering foil acquired through an iterative process produces an off-axis profile comparable to clinical measured data but is more representative of a 5 MeV electron beam when looking at the percent depth dose curve.

6. Conclusion

Creating an electron beam model within TOPAS through an iterative process by obtaining component sizes through open-source documents and comparing the data acquired to clinical data was determined to be feasible. The model created was based on the 6 MeV electron beam from the Elekta Versa HD, and the process could be used to develop other clinically relevant energies such as 8, 10, 12, and 15 MeV. Further investigation should be conducted to determine the source of the contamination causing peaks in the off-axis profile outside of the penumbral region, and more extensive history count simulations should be completed to produce plots with minimal noise.

7. References

1. Cancer Facts & Figures 2021. Published online 2021:72.

2. Khan FM, Gibbons JP. *Khan's the Physics of Radiation Therapy*. Fifth edition. Lippincott Williams & Wilkins/Wolters Kluwer; 2014.

3. Karzmark CJ. Advances in linear accelerator design for radiotherapy: Review Article: Advances in linear accelerator design. *Med Phys*. 1984;11(2):105-128. doi:10.1118/1.595617

4. Karzmark CJ, Morton RJ, Medical Physics Publishing Corporation. *A Primer on Theory and Operation of Linear Accelerators in Radiation Therapy.* Medical Physics Publishing; 1989.

5. McDermott PN, Orton CG. *The Physics & Technology of Radiation Therapy*. Second edition. Medical Physics Publishing; 2018.

6. Lax I, Brahme A. Collimation of High Energy Electron Beams. *Acta Radiol Oncol*. 1980;19(3):199-207. doi:10.3109/02841868009130153

7. Harrison RL, Granja C, Leroy C. Introduction to Monte Carlo Simulation. In: ; 2010:17-21. doi:10.1063/1.3295638

8. Razani A. A Monte Carlo Method for Radiation Transport Calculations. *J Nucl Sci Technol*. 1972;9(9):551-554. doi:10.1080/18811248.1972.9734896

9. Duderstadt JJ, Martin WR. *Transport Theory*. Wiley; 1979.

10. Lucas R, Roser R. *Transforming Geant4 for the Future*. U.S. Department of Energy; 2012:38. https://science.osti.gov/-/media/ascr/pdf/research/scidac/GEANT4-final.pdf

11. Perl J, Shin J, Schümann J, Faddegon B, Paganetti H. TOPAS: An innovative proton Monte Carlo platform for research and clinical applications: TOPAS: An innovative proton Monte Carlo platform. *Med Phys*. 2012;39(11):6818-6837. doi:10.1118/1.4758060

12. Kaluarachchi MM, Saleh ZH, Schwer ML, Klein EE. Validation of a Monte Carlo model for multi leaf collimator based electron delivery. *Med Phys*. 2020;47(8):3586-3599. doi:10.1002/mp.14194

13. Knöös T, Björk P, Nilsson P. Influence of initial electron beam characteristics on Monte Carlo calculated absorbed dose distributions for linear accelerator electron beams. *Phys Med Biol*. 2002;47(22):4019-4041. doi:10.1088/0031-9155/47/22/308

14. Bieda MR, Antolak JA, Hogstrom KR. The effect of scattering foil parameters on electron-beam Monte Carlo calculations. *Med Phys*. 2001;28(12):2527-2534. doi:10.1118/1.1420387

15. Harris GM. Development and validation of an electron Monte Carlo model for the Elekta Infinity accelerator. :172.

16. LeBlanc JD. Design of electron dual foil scattering systems for Elekta Infinity radiotherapy accelerators. :207.

17. Borzov E, Nevelsky A, Bar-Deroma R, Orion I. Dosimetric characterization of Elekta stereotactic cones. *J Appl Clin Med Phys*. 2018;19(1):194-203. doi:10.1002/acm2.12242

18. Patil BJ, Bhoraskar VN, Dhole SD. Optimization of Dual Scattering Foil for 6 to 20 MeV Electron Beam Radiotherapy. *N Y*. Published online 2011:3.

19. Karzmark CJ, Nunan CS, Tanabe E. *Medical Electron Accelerators*. McGraw-Hill, Inc., Health Professions Division; 1993.

20. Olsson M-L. Monte Carlo Simulation of the Elekta SLi Plus electron applicator system - A base for a new applicator design to reduce radiation leakage. Published online 2003.

21. Noshadi S, Atarod M, Amouheidari A, Felfeliyan F, Shokrani P. Evaluation of Therapeutic Properties of a Low Energy Electron Beam Plus Spoiler for Local Treatment of Mycosis Fungoides: A Monte Carlo Study. *J Biomed Phys Eng*. Published online August 20, 2017. doi:10.31661/jbpe.v0i0.712

8. Appendix

8.1. Iterative Process

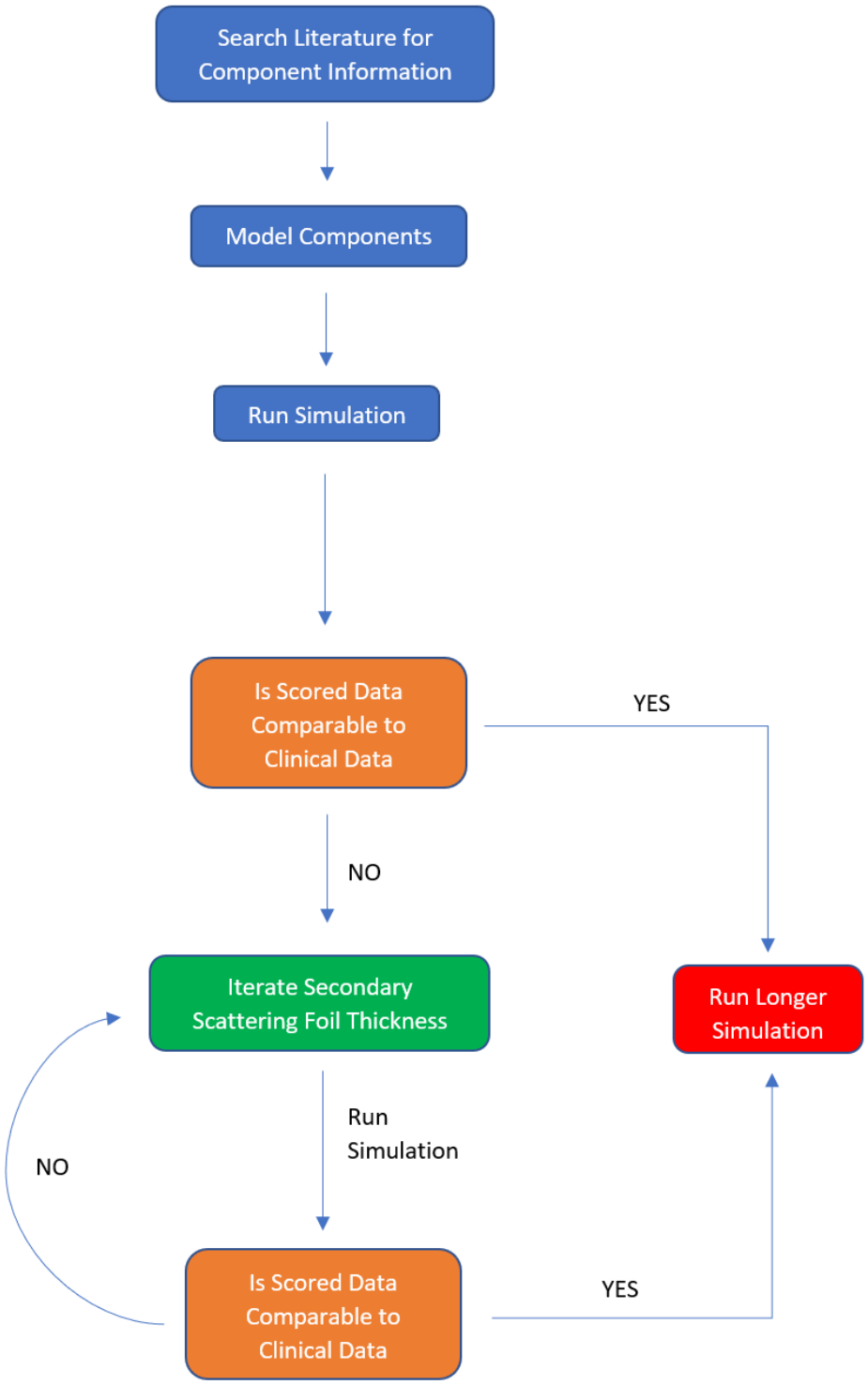

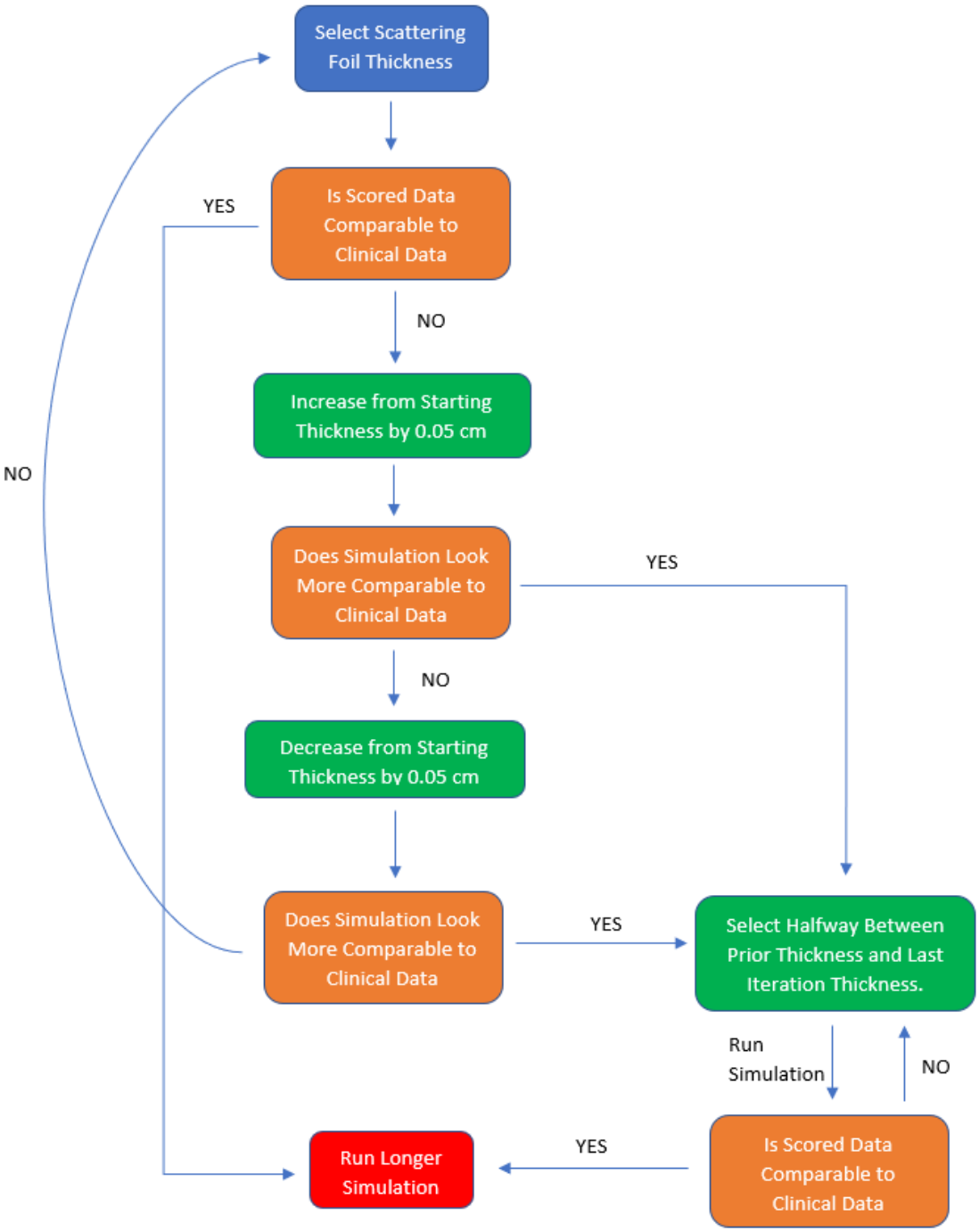
Select Scattering Foil Thickness
Is Scored Data Comparable to Clinical Data
YES
NO
Increase from Starting Thickness by 0.05 cm
NO
Does Simulation Look More Comparable to Clinical Data
YES
NO
Decrease from Starting Thickness by 0.05 cm
Does Simulation Look More Comparable to Clinical Data
YES
NO
Select Halfway Between Prior Thickness and Last Iteration Thickness.
Run Simulation
NO
Is Scored Data Comparable to Clinical Data
YES
Run Longer Simulation

8.2. Graphs

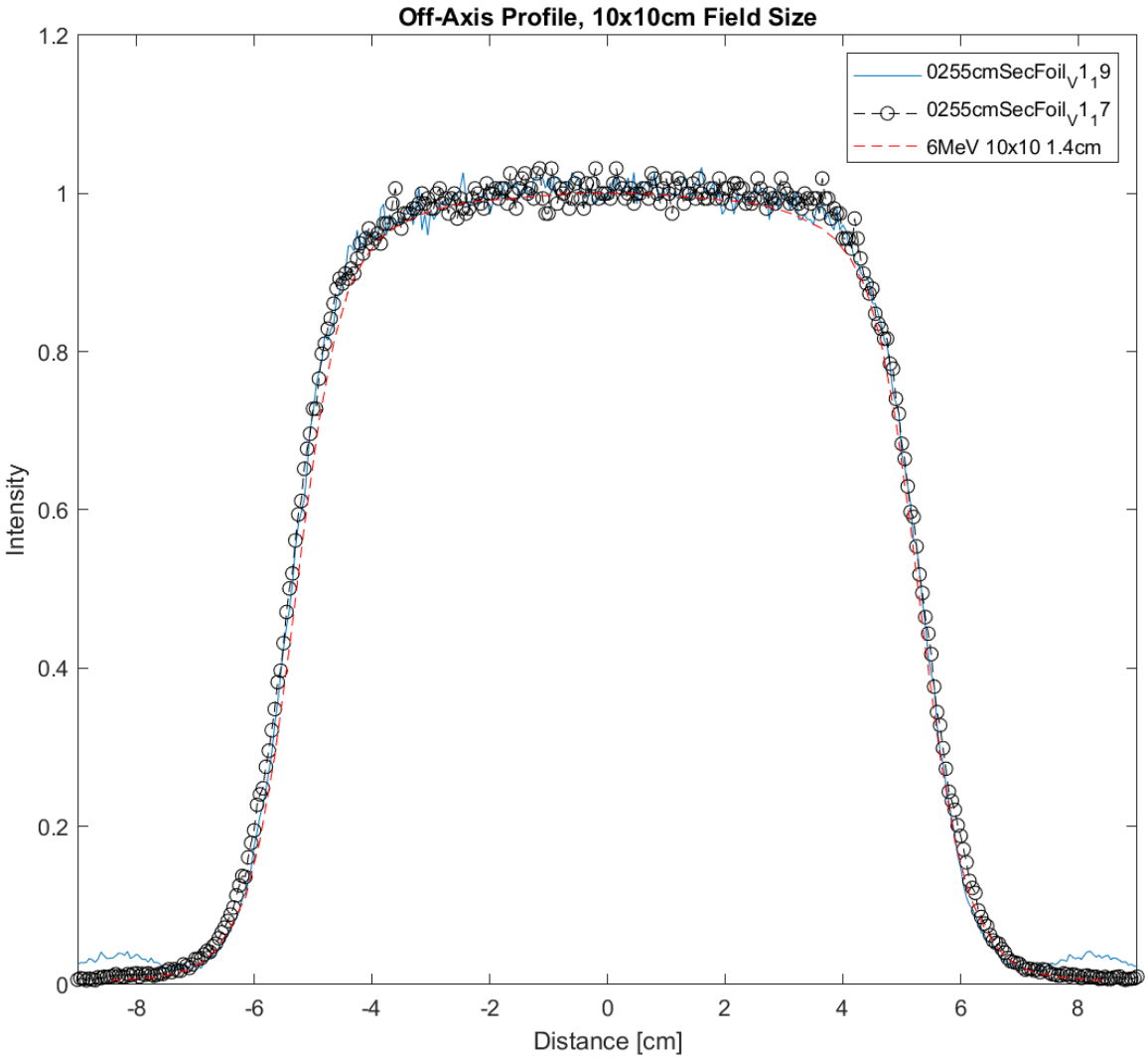

Figure 22. The graph between versions V1.17 and V1.19 where a new applicator system was created through the use of basic geometry figures built-in to the TOPAS software.

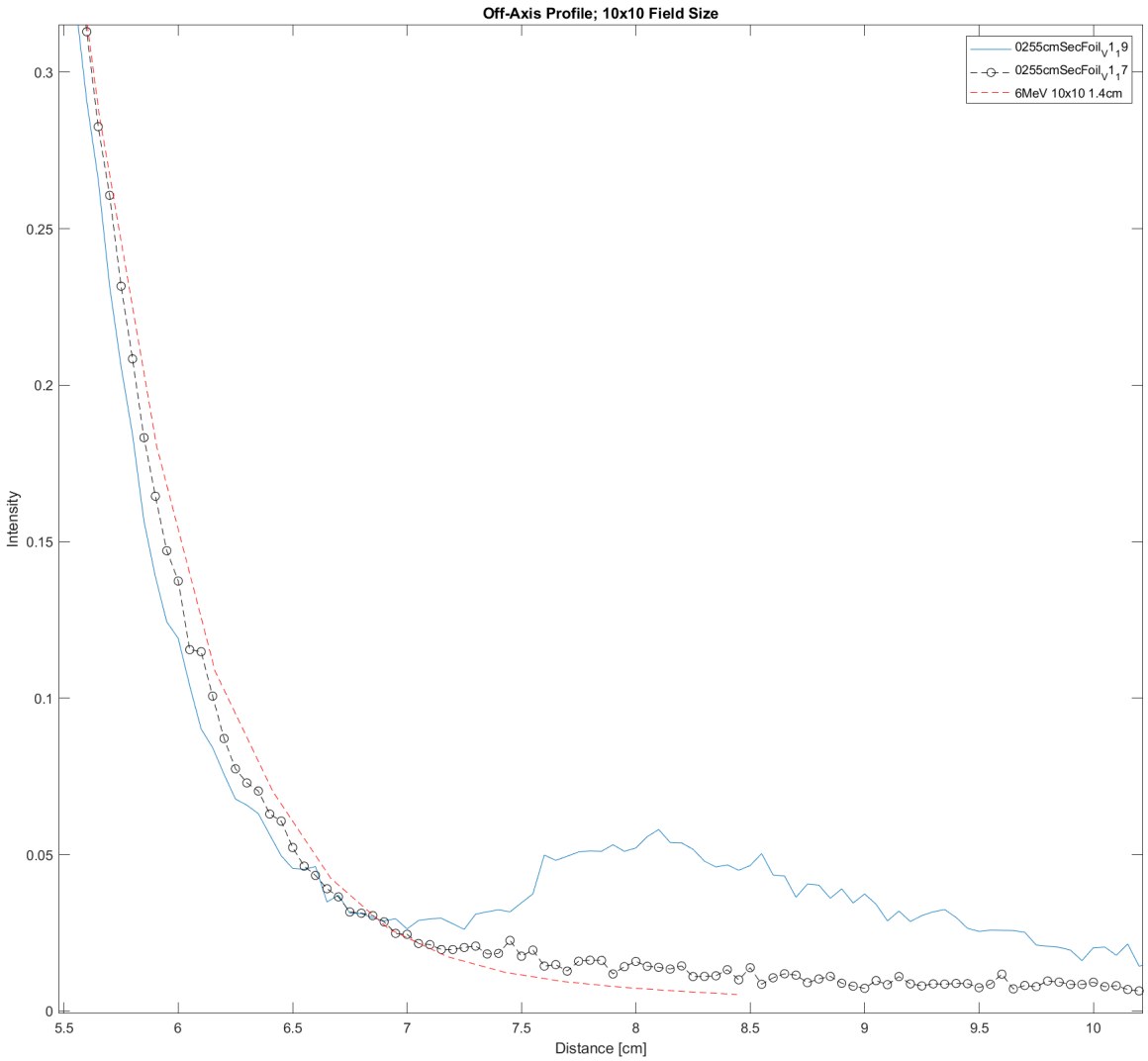

Figure 23. Zoomed in screenshot of the off-axis profiles between versions V1.17 and V1.19, where a new applicator system was created. This shows the spike in the off-axis profile located outside of the penumbral region.

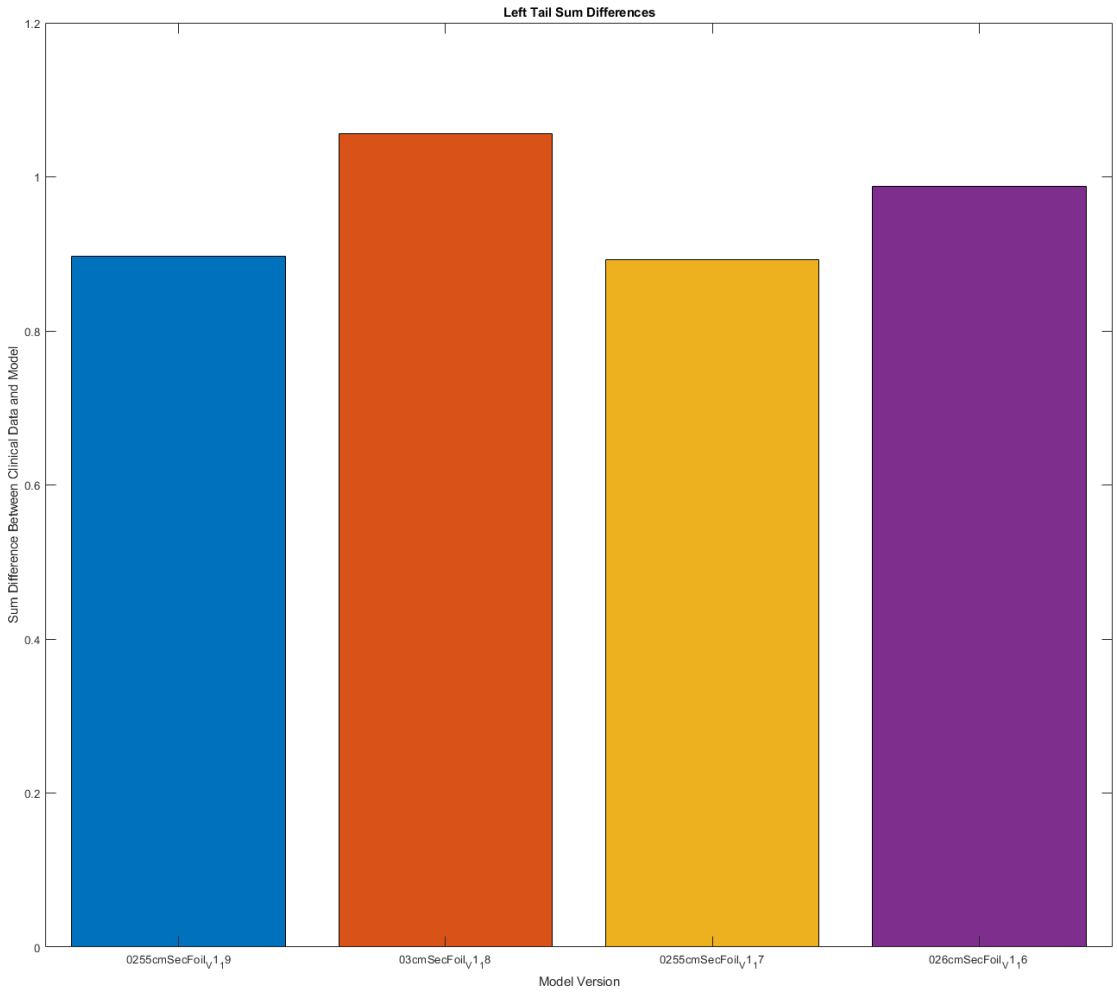

Figure 24. The total sum difference between each point of the simulation data and the clinical data within the tail of the off-axis profile between -11.3 and -5.8 cm for the 6 MeV energy electron beam at a depth of 0.95 cm and 10 by 10 field size.

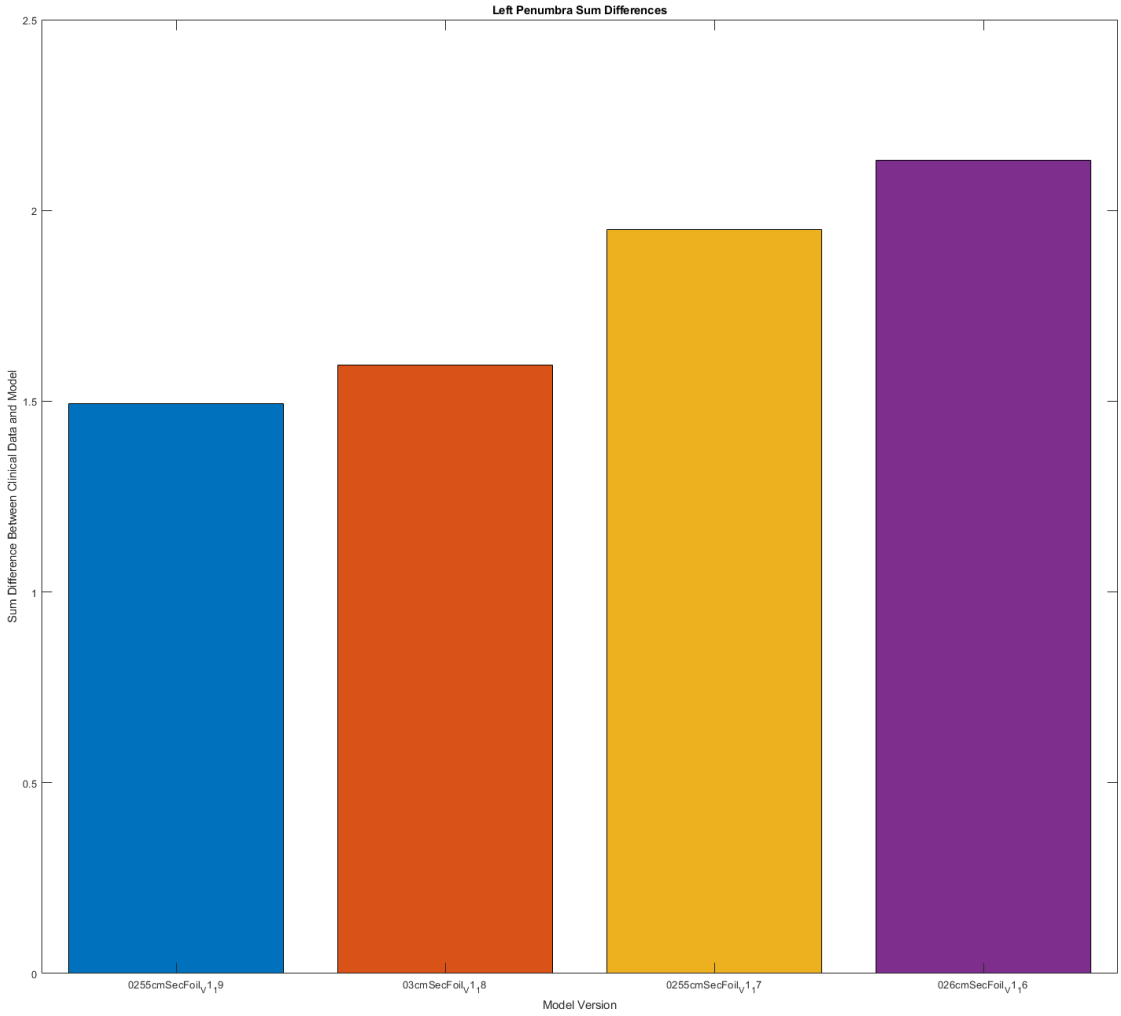

Figure 25. The total sum difference between each point of the simulation data and the clinical data within the penumbra of the off-axis profile between -5.8 and -4.85 cm for the 6 MeV energy electron beam at a depth of 0.95 cm and 10 by 10 field size.

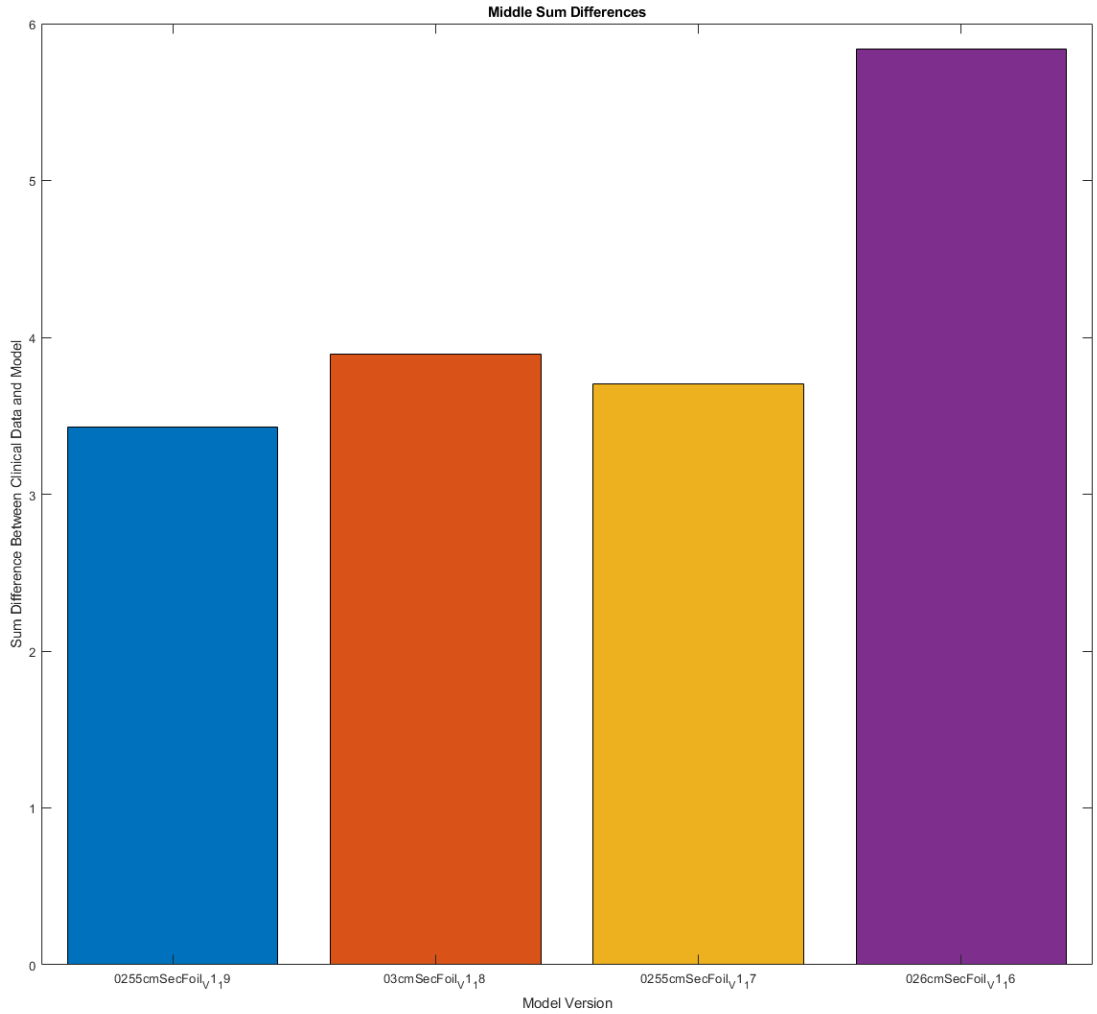

Figure 26. The total sum difference between each point of the simulation data and the clinical data within the middle section of the off-axis profile between -4.85 and 4.85 cm for the 6 MeV energy electron beam at a depth of 0.95 cm and 10 by 10 field size.

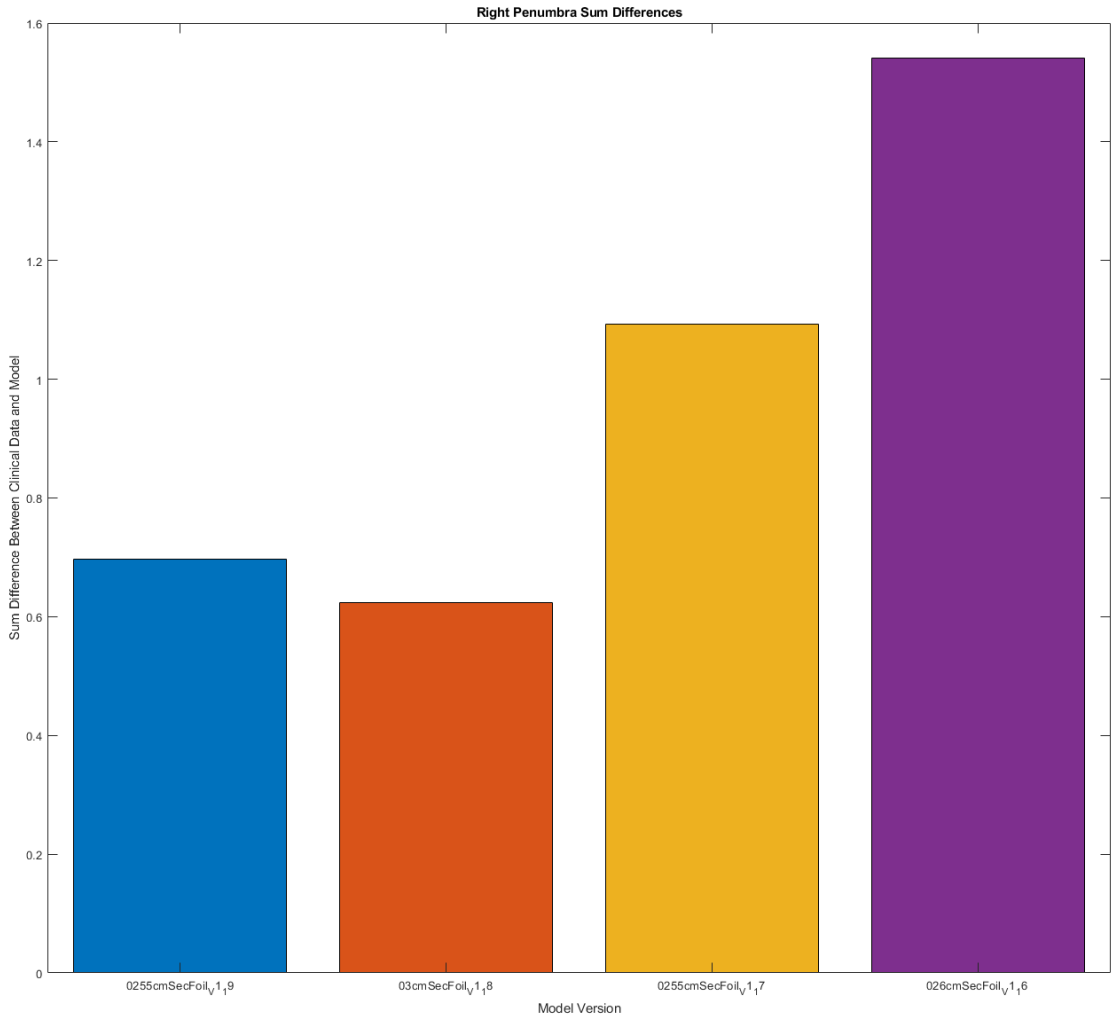

Figure 27. The total sum difference between each point of the simulation data and the clinical data within the penumbra of the off-axis profile between 4.85 and 4.75 cm for the 6 MeV energy electron beam at a depth of 0.95 cm and 10 by 10 field size.

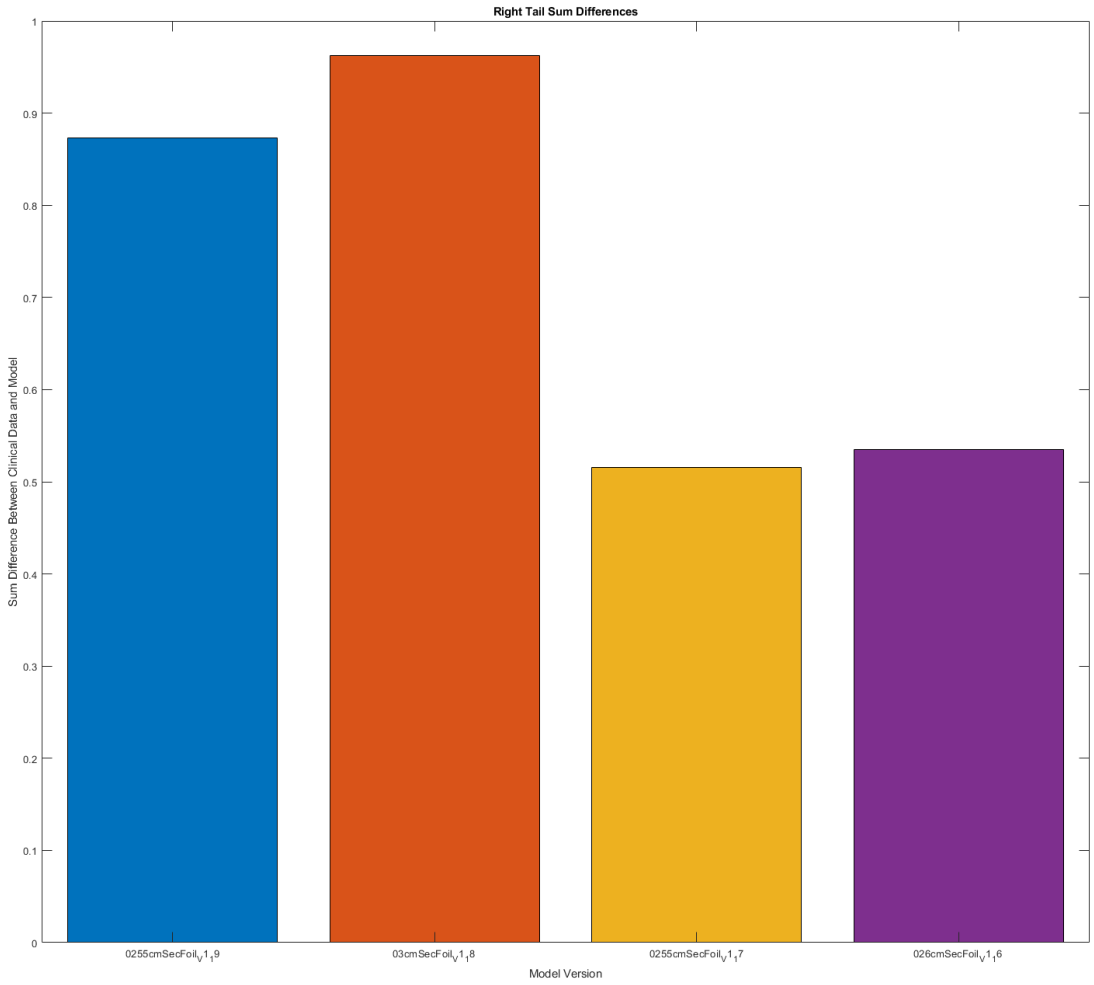

Figure 28. The total sum difference between each point of the simulation data and the clinical data within the tail of the off-axis profile between 4.75 and 11.3 cm for the 6 MeV energy electron beam at a depth of 0.95 cm and 10 by 10 field size.

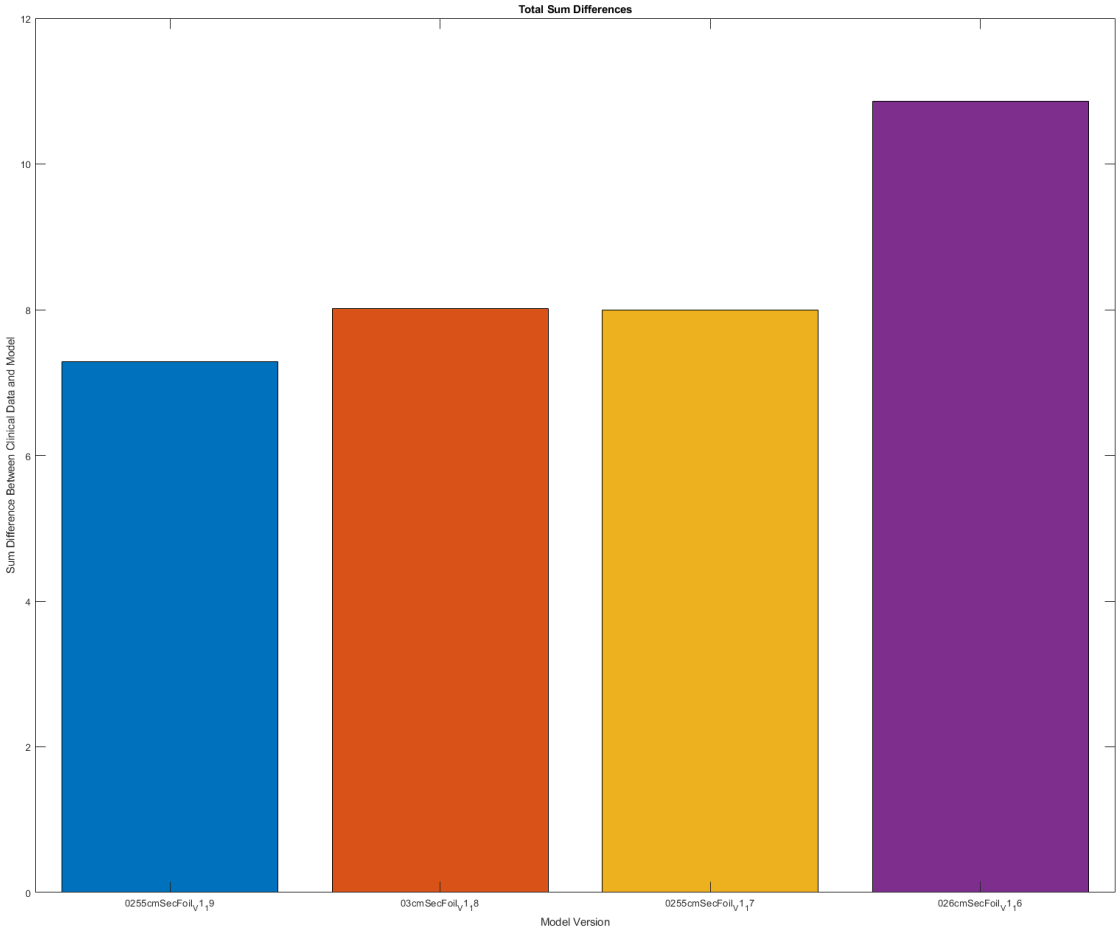

Figure 29. The total sum difference between each point of the simulation data and the clinical data within the off-axis profile for the 6 MeV energy electron beam at a depth of 0.95 cm and 10 by 10 field size.

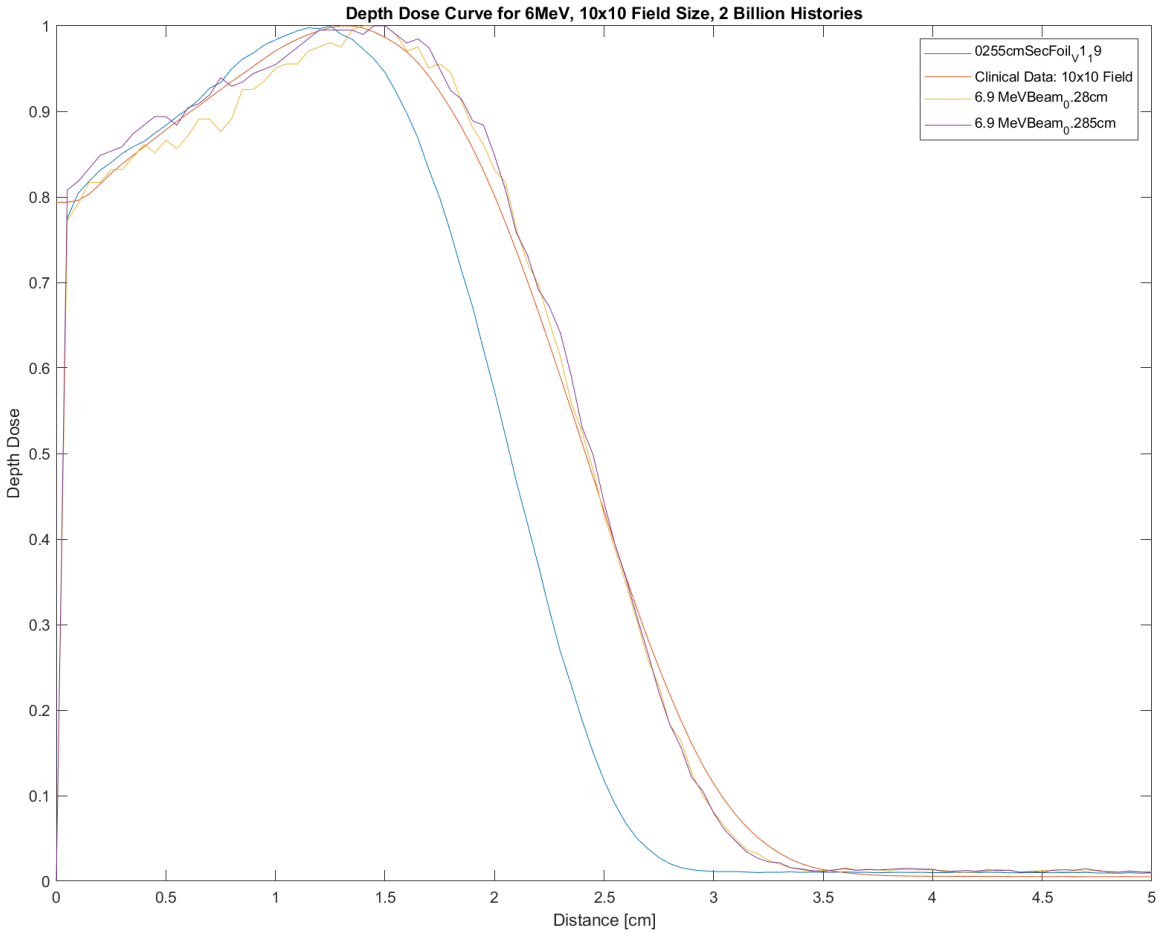

Figure 30. The percent depth dose curve for comparison of the 2 billion history count simulation for the final version of the model, which uses a 0.255-centimeter secondary scattering foil thickness, for a 10 by 10 cm^2 field size, the clinical measured data, and two new simulations utilizing a 6.9 MeV beam and different secondary scattering foil thicknesses.